

Genomic basis of geographical adaptation to soil nitrogen in rice

<https://doi.org/10.1038/s41586-020-03091-w>

Received: 22 March 2020

Accepted: 16 November 2020

Published online: 6 January 2021

 Check for updates

Yongqiang Liu^{1,2,7}, Hongru Wang^{1,7}, Zhimin Jiang¹, Wei Wang¹, Ruineng Xu^{3,4}, Qihui Wang⁵, Zhihua Zhang¹, Aifu Li^{1,2}, Yan Liang¹, Shujun Ou¹, Xiujie Liu^{1,2}, Shouyun Cao¹, Hongning Tong⁶, Yonghong Wang¹, Feng Zhou⁵, Hong Liao^{3,4}, Bin Hu^{1,5} & Chengcai Chu^{1,2,8}

The intensive application of inorganic nitrogen underlies marked increases in crop production, but imposes detrimental effects on ecosystems^{1,2}. It is therefore crucial for future sustainable agriculture to improve the nitrogen-use efficiency of crop plants. Here we report the genetic basis of nitrogen-use efficiency associated with adaptation to local soils in rice (*Oryza sativa* L.). Using a panel of diverse rice germplasm collected from different ecogeographical regions, we performed a genome-wide association study on the tillering response to nitrogen—the trait that is most closely correlated with nitrogen-use efficiency in rice—and identified *OsTCP19* as a modulator of this tillering response through its transcriptional response to nitrogen and its targeting to the tiller-promoting gene *DWARF AND LOW-TILLERING (DLT)*^{3,4}. A 29-bp insertion and/or deletion in the *OsTCP19* promoter confers a differential transcriptional response and variation in the tillering response to nitrogen among rice varieties. The allele of *OsTCP19* associated with a high tillering response to nitrogen is prevalent in wild rice populations, but has largely been lost in modern cultivars: this loss correlates with increased local soil nitrogen content, which suggests that it might have contributed to geographical adaptation in rice. Introgression of the allele associated with a high tillering response into modern rice cultivars boosts grain yield and nitrogen-use efficiency under low or moderate levels of nitrogen, which demonstrates substantial potential for rice breeding and the amelioration of negative environment effects by reducing the application of nitrogen to crops.

The application of nitrogen fertilizer has contributed considerably to crop yield and global food security, but causes serious environmental problems such as soil acidification and water eutrophication^{1,2}. It is therefore vital to improve crop nitrogen-use efficiency (NUE) to achieve a high yield with low nitrogen inputs⁵. However, modern breeding programmes have usually aimed at obtaining high yield under a high nitrogen supply, which has possibly resulted in a prevalence of low-NUE cultivars. Although NUE can be improved via field management⁶, genetic improvement to produce varieties with high NUE is a more fundamental strategy. The Asian cultivated rice is an economically important crop and is extremely diverse, with a large number of landraces that are cultivated in different eco-geographical regions. These varieties contain vital genetic variants that are important for their adaptation to their local environment (including soil fertility), which provides valuable genetic resource for breeding^{7–9}. Although several genetic variants that confer NUE variation have previously been identified in rice^{10–12}, the genetic basis of NUE in a more diverse and inclusive population remains largely unexplored. Here we have evaluated traits related to NUE in a panel

of diverse rice landraces, and identified a variant in the promoter of *OsTCP19* that is associated with the tillering response to nitrogen (TRN) through a genome-wide association study (GWAS). Moreover, the geographical distribution of *OsTCP19* alleles is closely associated with soil nitrogen content, which indicates that *OsTCP19* has an important role in adaptations to local soil conditions in different geographical regions.

Nitrogen-response evaluation in rice population

To investigate the genomic basis that underlies variation in NUE from a broad range of genetic diversity, we selected 110 rice accessions that have a similar growth period from the Rice Mini-Core Collection, a panel of diverse rice germplasm that has been collected worldwide by the US Department of Agriculture¹³. These accessions are mainly landraces that were collected from 52 countries and that cover all rice subgroups, including 20 tropical japonica, 10 temperate japonica, 28 aus, 30 indica, 3 aromatic and 19 admixed accessions¹³ (Fig. 1a, Extended Data Fig. 1a). The rapid linkage disequilibrium decay in this diverse population also

¹State Key Laboratory of Plant Genomics, Institute of Genetics and Developmental Biology, The Innovative Academy for Seed Design, Chinese Academy of Sciences, Beijing, China. ²College of Advanced Agricultural Sciences, University of Chinese Academy of Sciences, Beijing, China. ³State Key Laboratory for Conservation and Utilization of Subtropical Agro-bioresources, South China Agricultural University, Guangzhou, China. ⁴Root Biology Center, Haixia Institute of Science and Technology, Fujian Agriculture and Forestry University, Fuzhou, China. ⁵Sino-France Institute of Earth Systems Science, Laboratory for Earth Surface Processes, College of Urban and Environmental Sciences, Peking University, Beijing, China. ⁶National Key Facility for Crop Gene Resources and Genetic Improvement, Institute of Crop Sciences, Chinese Academy of Agricultural Sciences, Beijing, China. ⁷These authors contributed equally: Yongqiang Liu, Hongru Wang. ⁸e-mail: bhu@genetics.ac.cn; ccchu@genetics.ac.cn

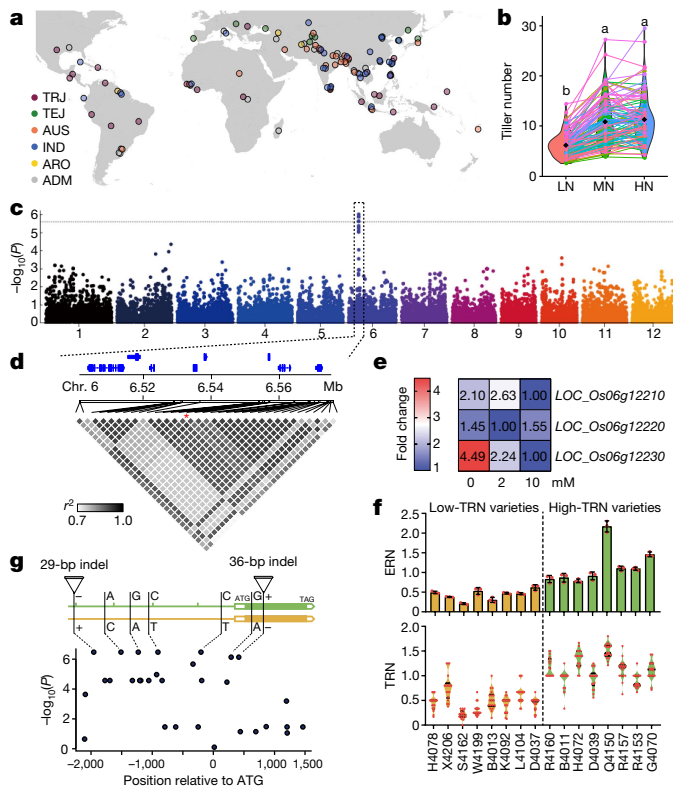


Fig. 1 | GWAS and fine mapping of the major locus that underlies TRN variation. **a**, Geographical distribution of 110 accessions. Each dot represents one variety. TRJ, tropical japonica; TEJ, temperate japonica; AUS, aus; IND, indica; ARO, aromatic; ADM, admixed. The map was made using the ‘maps’ package in R³². **b**, Tiller number of 110 accessions under low, moderate and high nitrogen conditions (LN, MN and HN, respectively). Dots represent the accessions; lines connect the same accession under different conditions. Black diamonds represent mean. Data are mean ($n=5$ plants). The significance analysis was performed according to one-way analysis of variance (ANOVA) and Tukey’s honest significant difference (HSD) test. Different letters indicate significant differences; for P values, see Source Data. **c**, Manhattan plot of GWAS for TRN. **d**, Linkage disequilibrium plot for SNPs with $P < 1.0 \times 10^{-5}$. Blue bars, genes. Asterisk, position of the peak SNP. The colour key (white to black) represents linkage disequilibrium values (r^2). **e**, A heat map of the relative expression of three candidate genes. The colour key (blue to red) represents gene expression (fragments per kilobase per million mapped reads (FPKM)) as fold change. For each gene, the lowest FPKM value was set as 1.00. **f**, Expression response to nitrogen (ERN) (the change of expression level relative to low expression level between different nitrogen conditions) of *OsTCP19* and the corresponding TRN values. For ERN, data are mean \pm s.d. of $n=3$ biologically independent samples. For TRN, $n=18$ plants; the bars within violin plots represent 25th percentiles, medians and 75th percentiles. **g**, Structure of *OsTCP19* and association mapping with more variants. Dots connected with the dashed lines indicate the seven variants that are significantly associated with TRN. x-axis, position relative to ATG (0 bp). In **c**, **g**, P values were determined under the mixed linear model using Wald test, implemented in GEMMA.

allows the mapping of associations to a relatively narrow genomic region (Extended Data Fig. 1b).

The responsiveness of grain yield to nitrogen fertilization is the index that is most frequently used for NUE¹⁴. In rice, the tiller number (the number of panicles per plant), grain number per panicle and grain weight directly determine grain yield and thus can closely reflect NUE. We evaluated the response to nitrogen of these agronomic traits in the field under three nitrogen regimes: low nitrogen (50 kg ha⁻¹), moderate nitrogen (150 kg ha⁻¹) and high nitrogen (300 kg ha⁻¹). Tiller number displayed a significant positive response to increasing nitrogen from low to moderate nitrogen for all varieties in the population, but was

less sensitive from moderate to high nitrogen (Fig. 1b). However, grain number per panicle and 1,000-grain weight displayed an inconsistent response to increasing nitrogen among different varieties (Extended Data Fig. 1c, d). The nitrogen response was further calculated with the value of (moderate nitrogen – low nitrogen)/low nitrogen, and TRN showed the highest responsiveness value and the largest variance among different varieties (Extended Data Fig. 1e, f); this indicated that TRN might be an ideal index for phenotyping NUE to carry out a GWAS.

Identification of TRN-associated genomic variants

Using a mixed linear model for GWAS, we identified a major peak on chromosome 6, in which the top single-nucleotide polymorphism (SNP) (chromosome 6: 6555157) was highly associated with TRN ($P = 9.46 \times 10^{-7}$), and this peak explained about 20% of the phenotypic variation (Fig. 1c). Linkage disequilibrium analysis on the peak region showed that the top SNP is located within an approximately 20-kb block (Fig. 1d). This linkage disequilibrium block spanned three genes: *LOC_Os06g12210*, *LOC_Os06g12220* and *LOC_Os06g12230*. Using a relatively strict P value threshold ($P < 1.5 \times 10^{-6}$), we identified 15 SNPs that are significantly associated with TRN in this peak: one SNP is close to *LOC_Os06g12210*, two SNPs are close to *LOC_Os06g12220* and 12 SNPs are close to *LOC_Os06g12230* (Extended Data Fig. 1g, Supplementary Table 1). Given their association with nitrogen response, we first examined the transcript expression of these three candidate genes in response to nitrogen. Only *LOC_Os06g12230* (known as *OsTCP19*)¹⁵ displayed an obvious nitrogen-repressed expression pattern in the root (Fig. 1e, Extended Data Fig. 1h), and the expression of this gene was related more to nitrate than ammonium (Extended Data Fig. 1i). In addition, high-TRN varieties displayed a stronger negative response to nitrogen in *OsTCP19* expression than that of low-TRN varieties in the root, which is in accordance with their TRN values (Fig. 1f, Extended Data Fig. 2a, b). Thus, *OsTCP19* might be the causal gene that underlies variation in the TRN. We also detected the expression of three candidate genes in response to nitrogen in the shoot base, the tissue in which tiller buds initiate, in both high-TRN and low-TRN varieties. Nonetheless, the expression of these three genes did not display a substantial response to nitrogen in the shoot base (Extended Data Fig. 3), which suggests a possible mobile signal from the root to the shoot base to modulate tillering.

To fully resolve the DNA sequence variation in *OsTCP19* that might have been missed by low-coverage genome sequencing¹³, we resequenced *OsTCP19* and conducted an association analysis with the variants we identified (Supplementary Table 2). One insertion and/or deletion (indel) (-2009, 29-bp; referred to as v3) and four SNPs (-1605C>A, -1347A>G, -1054T>C and -414T>C; referred to as v6, v8, v13 and v20, respectively) in the promoter region of *OsTCP19* show a stronger association signal with TRN ($P = 3.34 \times 10^{-7}$) than does the top SNP (Fig. 1g). In addition, we also detected one SNP (+35A>G; referred to as v24) and one indel (+148, 36-bp; referred to as v26) in the coding sequence that show significant associations with TRN ($P = 7.29 \times 10^{-7}$) (Fig. 1g, Supplementary Table 2).

OsTCP19 negatively regulates rice tillering

OsTCP19 encodes a plant-specific transcription factor of the TEO-SINTE BRANCHED 1, CYCLOIDEA AND PROLIFERATING CELL FACTOR (TCP) family^{15,16} (Extended Data Fig. 4a). *OsTCP19* was predominantly localized to the nucleus and highly expressed in the root and shoot base (Fig. 2a, b). We further generated lines that overexpress *OsTCP19* (lines TO1 and TO2) as well as lines in which *OsTCP19* is inhibited by RNA interference (T-Ri1 and T-Ri2). For generating lines that overexpress *OsTCP19*, we introduced an *OsTCP19* genomic DNA fragment containing the promoter and gene body regions into the japonica variety Zhonghua 11 (ZH11). The *OsTCP19*-overexpression lines showed

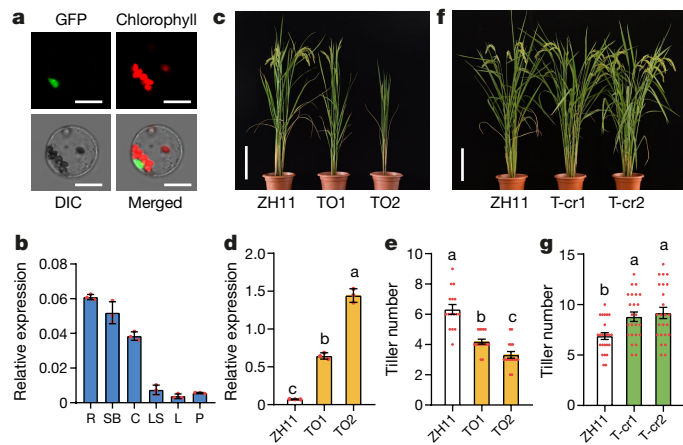


Fig. 2 | *OsTCP19* negatively regulates rice tillering. **a**, Subcellular localization of *OsTCP19*-GFP fusion protein in rice protoplasts. Scale bars, 10 μ m. The results are representative of three independent experiments. DIC, differential interference contrast. **b**, Quantitative PCR with reverse transcription (qRT-PCR)-based transcript abundance analysis of *OsTCP19* in various tissues. R, roots; SB, shoot bases; C, culms; L, leaves; LS, leaf sheaths; P, panicles. Data are mean \pm s.d. ($n=3$ biologically independent samples). **c**, Phenotype of ZH11, TO1 and TO2 lines. Scale bar, 24 cm. **d**, Expression analysis of *OsTCP19* in ZH11, TO1 and TO2 lines. Data are mean \pm s.d. ($n=3$ biologically independent samples). **e**, Tiller number per plant of ZH11, TO1 and TO2 lines. Data are mean \pm s.e.m. ($n=16$ plants). **f**, Phenotype of ZH11, T-cr1 and T-cr2 plants. Scale bar, 24 cm. **g**, Tiller number of ZH11, T-cr1 and T-cr2 plants. Data are mean \pm s.e.m. ($n=24$ plants). In **d**, **e**, **g**, different letters indicate significant differences ($P<0.05$, one-way ANOVA, Tukey's HSD test); for *P* values, see Source Data.

a significantly reduced tiller number as compared with wild-type ZH11 plants (Fig. 2c–e). We also introduced the coding sequence of *OsTCP19* driven by CaMV 35S promoter into the ZH11 variety to generate constitutive *OsTCP19*-overexpression (cTO) lines. The cTO lines also displayed decreased tiller number as well as a repressed TRN (Extended Data Fig. 4b–e). By contrast, plants in which *OsTCP19* is inhibited by RNA interference exhibited a significant increase in tiller number (Extended Data Fig. 4f–h). Additionally, plants of two CRISPR–Cas9-based knockout lines (T-cr1 and T-cr2) also generated more tillers (Fig. 2f, g, Extended Data Fig. 4i). These results indicate that *OsTCP19* acts as a negative regulator of tillering in rice.

Indel in *OsTCP19* promoter confers TRN variation

Using the variants identified in *OsTCP19*, we classified the gene allelic variations into two haplotypes: one associated with high-TRN varieties (haplotype H (*OsTCP19*-H)) and one with low-TRN varieties (haplotype L (*OsTCP19*-L)) (Fig. 3a, b). Among 110 accessions of Rice Mini-Core Collection, almost all the aus varieties (96.4%) belong to *OsTCP19*-H, whereas almost all the japonica (100% of the temperate japonica and 95% of the tropical japonica) and most indica (76.7%) varieties belong to *OsTCP19*-L (Supplementary Table 3). We further constructed a near-isogenic line (NIL) that carries the *OsTCP19*-H allele from the aus variety Kasalath (Kasa) in the background of the japonica variety Koshihikari (Kos) (Extended Data Fig. 5a). Compared to Kos, NIL *OsTCP19*-H plants showed a greater negative response to nitrogen in *OsTCP19* expression as well as higher TRN (Fig. 3c–e). The *OsTCP19*-H promoter displayed a more-significant activity-decline rate in response to nitrogen treatment, which is consistent with the stronger negative response to nitrogen in *OsTCP19*-H transcript expression (Fig. 3f). To pinpoint the functional mutation, we mutated the *OsTCP19*-L promoter by introducing each of five variations from the *OsTCP19*-H promoter (Fig. 3a). The nitrogen repression rate of the activity of the *OsTCP19*-L promoter was significantly enhanced by deleting the 29-bp indel, to a

level that was comparable to that of the *OsTCP19*-H promoter (Fig. 3f). By contrast, none of the other four SNP mutations could enhance the nitrogen repression rate of the activity of the *OsTCP19*-L promoter (Fig. 3f). Moreover, we generated gene-edited plants with a deletion at this 29-bp indel region in ZH11 (*OsTCP19*-L type) (Extended Data Fig. 5b). The *OsTCP19*-L gene-edited (TGE) plants displayed a more significant negative response to nitrogen in *OsTCP19* expression as well as higher TRN (Extended Data Fig. 5c–g), which further confirms that the 29-bp indel in the promoter is the causal variant.

We identified two binding sites of LATERAL ORGAN BOUNDARIES DOMAIN (LBD) proteins, the transcriptional repressors of nitrogen responses¹⁷, in the flanking sequence of the 29-bp indel (Extended Data Fig. 5h, Supplementary Table 4). We further identified two nitrogen-inducible LBD proteins (*OsLBD37* and *OsLBD39*) that are clustered most closely to previously characterized LBD proteins in *Arabidopsis*¹⁸ (Extended Data Fig. 5i, j). The expression of *OsTCP19* was significantly repressed in *OsLBD37*- and *OsLBD39*-overexpression plants (Extended Data Fig. 5k–n), and the LBD proteins repressed the promoter activity of both *OsTCP19*-L and *OsTCP19*-H (although they exhibited a more significant repression of *OsTCP19*-H) (Fig. 3g). In particular, in the absence of the 29-bp indel sequence, *OsTCP19*-L showed a significantly enhanced repression by LBD proteins (Fig. 3g). These results indicate that the 29-bp indel in the promoter can affect the repression effect of LBD proteins to the *OsTCP19* promoter. Additionally, two variants in *OsTCP19* coding region showed the same protein subcellular localization and a similar effect in repressing tillering (Extended Data Fig. 6a–d), which suggests that they do not affect the protein function. These results together demonstrate that the 29-bp indel in the promoter region of *OsTCP19* alters its transcriptional expression in response to nitrogen, thereby conferring divergence in TRN in different rice varieties.

OsTCP19–*DLT* module underlies TRN regulation

Using RNA-seq profiling generated from wild-type (ZH11) and *OsTCP19*-overexpressing plants (TO1 and TO2), we identified 2,993 differentially expressed genes (DEGs). We retained 822 DEGs that were annotated in development-related processes in Gene Ontology analysis. Of these, we identified 304 DEGs as the potential target genes of *OsTCP19* after TCP-binding *cis*-element screening in the promoter region (Extended Data Fig. 7a, b, Supplementary Data 1). Given that the transcript expression of *OsTCP19* is tightly regulated by nitrogen, its target genes should be also regulated by nitrogen in a correlation with *OsTCP19*. We therefore generated an *OsTCP19*-correlated nitrogen-responsive gene set on the basis of nitrogen-treated RNA-seq analysis (Supplementary Data 1). By overlapping the 304 DEGs with this nitrogen-responsive gene set, we obtained 15 potential target genes (Fig. 4a). Among them, *DLT* has previously been shown to have important roles in regulating brassinosteroid signalling and promoting tillering in rice^{3,4}, which makes it a vital downstream component of *OsTCP19* in modulating tillering. *DLT* expression was greatly repressed in *OsTCP19*-overexpressing plants, but was upregulated in *OsTCP19* knock-out mutants (Extended Data Fig. 7c). In addition, yeast one-hybrid assays combined with *DLT*_{promoter}–*LUC* assays in rice protoplasts suggested that *OsTCP19* could directly bind to and repress the activity of the *DLT* promoter (Fig. 4b, Extended Data Fig. 7d). Chromatin immunoprecipitation with quantitative PCR (ChIP-qPCR) assays showed that both *OsTCP19*-L and *OsTCP19*-H were significantly enriched in the predicted binding sites of the *DLT* promoter (Extended Data Fig. 7e). Furthermore, gel electrophoresis mobility shift assay (EMSA) demonstrated that both *OsTCP19*-L and *OsTCP19*-H markedly reduced the migration of the probe that contains the predicted binding sites of the *DLT* promoter (Fig. 4c), which indicates that *OsTCP19* can directly bind to the *DLT* promoter.

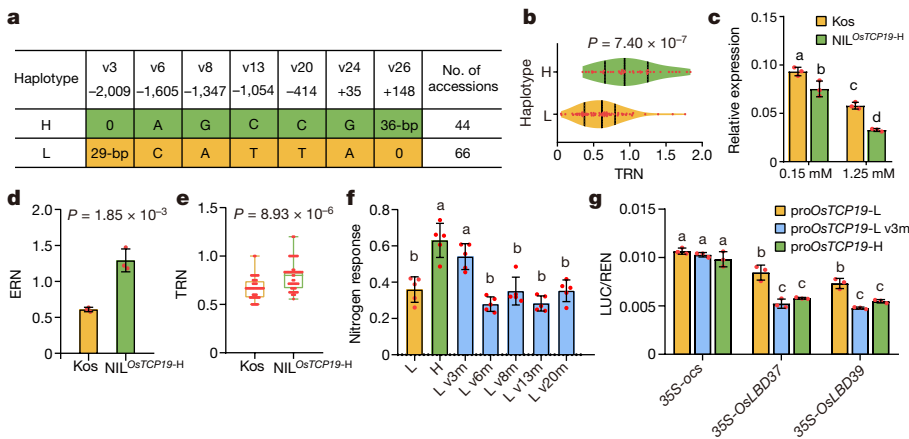


Fig. 3 | Indel of 29 bp in the *OsTCP19* promoter confers different nitrogen responses. **a**, Major haplotypes of *OsTCP19*. v3, v6, v8, v13, v20, v24 and v26 indicate the variants, and their positions relative to ATG are shown in the table. **b**, TRN distribution between haplotype H ($n=44$ accessions) and haplotype L ($n=66$ accessions). The bars within violin plots represent 25th percentiles, medians, and 75th percentiles. **c**, Expression of *OsTCP19* in Kos and *NIL^{OsTCP19-H}* grown under 0.15 mM and 1.25 mM NH_4NO_3 . Data are mean \pm s.d. ($n=3$ biologically independent samples). **d**, ERN of *OsTCP19* generated from **c**. Data are mean \pm s.d. ($n=3$ biologically independent samples). **e**, TRN of Kos and *NIL^{OsTCP19-H}*. $n=52$ plants. The horizontal bars of boxes represent minima, 25th

percentiles, medians, 75th percentiles and maxima. **f**, Nitrogen response analysis of different variations in *OsTCP19* promoter. v3m, v6m, v8m, v13m and v20m represent the mutations introduced into the promoter of *OsTCP19-L*. Data are mean \pm s.d. ($n=5$ biologically independent samples). **g**, Indel of 29 bp resulted in divergent repression of LBD proteins to *OsTCP19* promoter, as shown by firefly luciferase/*Renilla* luciferase activity ratio (LUC/REN). Data are mean \pm s.d. ($n=3$ biologically independent samples). In **b**, **d**, **e**, significant difference was determined by two-sided Student's *t*-test. In **c**, **f**, **g**, different letters indicate significant differences ($P<0.05$, one-way ANOVA, Tukey's HSD test); for *P* values, see Source Data.

DLT displayed a similar tissue expression pattern and an opposite nitrogen-responsive expression pattern to those of *OsTCP19* (Extended Data Fig. 7f, g). Besides low tillering, *OsTCP19*-overexpression lines exhibited typical brassinosteroid-deficient phenotypes, including reduced plant height, erected and dark-green leaves, and shortened panicles, which highly resembled the phenotypes of *dlt*-mutant plants (Fig. 4d, e, Extended Data Fig. 7h, i). Both *OsTCP19*-overexpressing and *dlt*-mutant plants showed a decreased sensitivity to brassinosteroid³ (Extended Data Fig. 7j, k). In addition, overexpression of *DLT* rescued the low tillering as well as other brassinosteroid-deficient phenotypes of *OsTCP19*-overexpressing plants (Fig. 4f–h, Extended

Data Fig. 7l, m). Moreover, the expression of *DLT* was well-correlated with *OsTCP19* in high-TRN and low-TRN varieties, consistent with TRN variation among different varieties (Extended Data Fig. 7n, o). In the *NIL^{OsTCP19-H}* line, the expression of *DLT* was also significantly increased (Extended Data Fig. 7p). These results demonstrate that *OsTCP19* can directly target *DLT* and repress its transcript expression, thus negatively modulating tillering. Furthermore, we found that tiller bud outgrowth—but not initiation—is repressed in *OsTCP19*-overexpressing and *dlt*-mutant plants (Extended Data Fig. 8a–d). The expression of key cell-cycle marker genes^{19,20} was also suppressed in the shoot base of *OsTCP19*-overexpressing and *dlt*-mutant plants, which indicates that

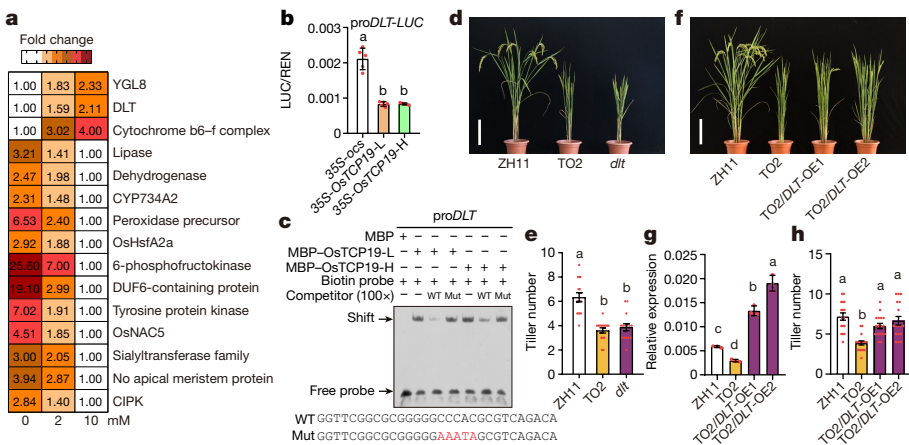


Fig. 4 | DLT works downstream of *OsTCP19*. **a**, The relative expression of 15 DEGs. The colour key (white to brown) represents gene expression (FPKM) as fold changes. For each gene, the lowest FPKM value was set as 1.00. The gene-encoding proteins are shown on the right. **b**, *OsTCP19* displays repression activity to *DLT*_{promoter}-*LUC* (pro*DLT*-*LUC*) in rice protoplasts. Data are mean \pm s.d. ($n=5$ biologically independent samples). **c**, *OsTCP19* directly binds to the *DLT* promoter in EMSA. One-hundred-fold unlabelled wild type (WT) or mutation (mut) probes were used for competition. The probe sequences are listed below and mutated sequence is shown in red. The results are representative of three independent experiments (Supplementary Fig. 1). MBP, maltose-binding

protein. **d**, Phenotype of ZH11, TO2 and *dlt* plants. Scale bar, 24 cm. **e**, Tiller number per plant of ZH11, TO2 and *dlt* lines. Data are mean \pm s.e.m. ($n=15$ plants). **f**, Phenotype of ZH11, TO2 and *DLT*-overexpression lines in the TO2 background (TO2/*DLT*-OE1 and -OE2). Scale bar, 24 cm. **g**, Expression analysis of *DLT* in ZH11, TO2 and TO2/*DLT*-overexpression lines. Data are mean \pm s.d. ($n=3$ biologically independent samples). **h**, Tiller number per plant of ZH11, TO2 and TO2/*DLT*-overexpression lines. Data are mean \pm s.e.m. ($n=17$ plants). In **b**, **e**, **g**, **h**, different letters indicate significant differences ($P<0.05$, one-way ANOVA, Tukey's HSD test); for *P* values, see Source Data.

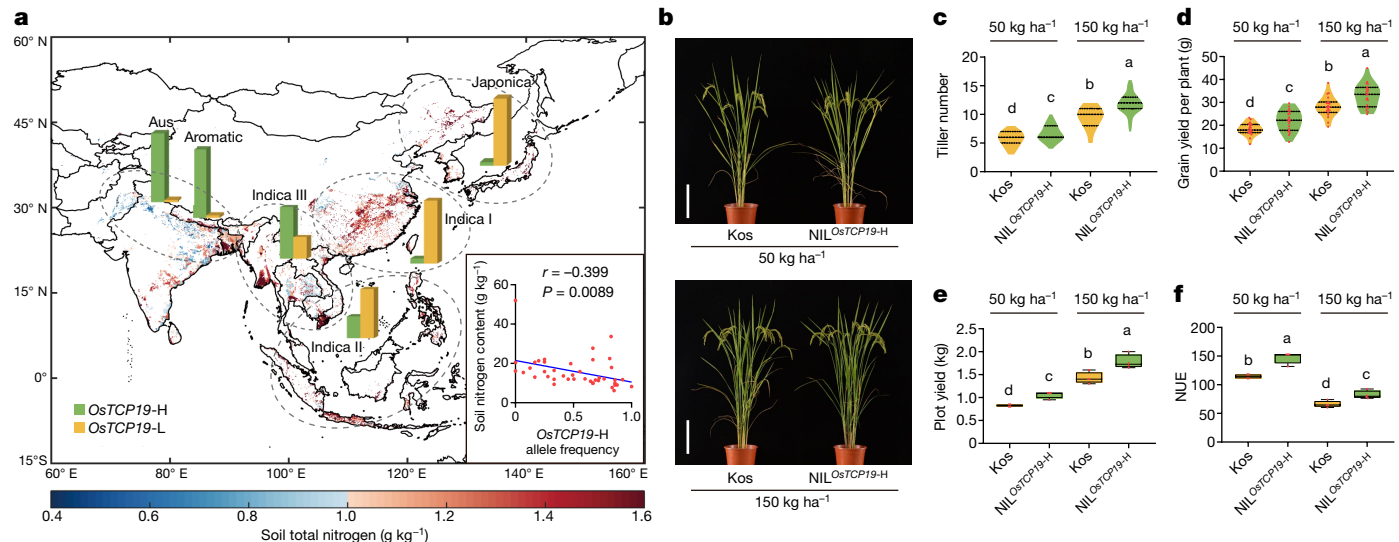


Fig. 5 | *OsTCP19-H* contributes to the geographical adaptation and significantly increases the NUE of modern cultivars. **a**, *OsTCP19-H* frequency is highly correlated with soil nitrogen content. Main plot, geographical distribution of soil nitrogen content and *OsTCP19* allele frequency among different subgroups of rice in Asia. The colour key (blue to red) represents soil total nitrogen content (g kg^{-1}). Different rice types include japonica ($n = 874$ accessions), indica I ($n = 205$ accessions), indica II ($n = 217$ accessions), indica III ($n = 891$ accessions), aromatic ($n = 81$ accessions) and aus ($n = 201$ accessions). Inset, Pearson correlation coefficient analysis of *OsTCP19-H* allele frequency with soil total nitrogen content in 42 countries or regions worldwide. The map was generated in MATLAB R2016b (MATLAB and Statistics Toolbox Release R2016b, The MathWorks). The base map of the

country boundaries was from the ArcGIS Hub (ESRI; ‘Countries WGS84’ shapefile). Global scale. ‘ArcGIS Hub’. 2015.06.21). **b**, Phenotype of Kos and *NIL_OsTCP19-H* plants grown under two nitrogen conditions in Beijing in 2019. Scale bars, 24 cm. **c–f**, Statistical analysis of Kos and *NIL_OsTCP19-H* plants under two nitrogen conditions. Tiller number (**c**) ($n = 52$ plants), grain yield per plant (**d**) ($n = 20$ plants), plot yield (**e**) ($n = 4$ plots) and NUE (**f**) ($n = 4$ plots) of Kos and *NIL_OsTCP19-H*. In **c**, **d**, the bars in the violin plots represent 25th percentiles, medians, and 75th percentiles. In **e**, **f**, the horizontal bars of boxes represent minima, 25th percentiles, medians, 75th percentiles and maxima. In **c–f**, different letters indicate significant differences ($P < 0.05$, one-way ANOVA, Tukey’s HSD test); for P values, see Source Data.

OsTCP19-DLT modulates tiller bud outgrowth by regulating cell division (Extended Data Fig. 8e). Previous studies have also revealed that both nitrogen and brassinosteroid promote rice tillering by modulating tiller bud outgrowth^{12,21,22}. Our findings here thus suggest integrated nitrogen–brassinosteroid signalling for modulating rice tillering by the *OsTCP19-DLT* module. Indeed, brassinosteroid-promoted tillering was greatly repressed in both *OsTCP19*-overexpressing and *dlt*-mutant plants (Extended Data Fig. 8f, g), further supporting this hypothesis.

Geographical distribution of *OsTCP19* allele

Haplotype analysis from 110 accessions of the Rice Mini-Core Collection revealed that *OsTCP19-L* is enriched in japonica and indica rice, whereas *OsTCP19-H* is predominantly found in aus and aromatic rice. We then extended this analysis to 3,024 rice accessions from the 3K Rice Genomes Project²³. We identified 20 unique high-confidence haplotypes, and assigned 13 out of the 20 haplotypes to the *OsTCP19-H* haplotype group; the rest were assigned to the *OsTCP19-L* haplotype group (Supplementary Table 5). Of the accessions from the 3K Rice Genomes Project, 94% of aus and 93.8% of aromatic varieties contained the *OsTCP19-H* allele, whereas only 4.9% of japonica varieties contained this allele (Supplementary Table 6). The frequency of occurrence of the *OsTCP19-H* allele was highly variable in indica varieties, at 68.7% in indica III, 29.5% in indica II and only 7.3% in indica I (Supplementary Table 6). This led us to speculate whether the allele distribution of *OsTCP19* in different rice subgroups contributes to their environmental adaptation, especially the soil nitrogen content in different geographical locations. We then collected data of soil total nitrogen content in rice planting areas from 42 countries or regions. When projecting all varieties back to their original locations²⁴, we observed a strong association between *OsTCP19-H* allele frequency and soil nitrogen content (Fig. 5a). Notably, nitrogen-poor regions are mainly distributed in the

northeastern India and Bangladesh along the basin of the Ganges River, where the aus varieties originated and *OsTCP19-H* is highly prevalent²⁵ (Fig. 5a). By contrast, in nitrogen-rich regions (including northern China, Korea and Japan) where japonica varieties are widely cultivated, the *OsTCP19-H* has nearly been lost (Fig. 5a). Meanwhile, indica varieties—which show a variable allele frequency of *OsTCP19-H*—span regions from Southeast Asia to southern China that have varied soil nitrogen content (Fig. 5a). To exclude the possibility that this effect was the result of different genetic backgrounds, we performed a correlation test using only indica varieties. Indeed, *OsTCP19-H* allele frequency showed a significant negative correlation with soil nitrogen content ($r = -0.399, P = 0.0089$) (Fig. 5a). This result was further confirmed by excluding the effects of other environmental factors, such as atmospheric temperature and dryness (Extended Data Fig. 9a–d). These findings indicate that the *OsTCP19-H* allele might have contributed to the geographical adaptation of rice varieties to nitrogen-poor soil. All of the wild rice subgroups—including both *Oryza rufipogon* I (which is closely related to aus and indica) and *O. rufipogon* III (which is related to japonica)²⁶—possessed an extremely high allele frequency of *OsTCP19-H* (over 90%) (Supplementary Table 7). These results suggest that the *OsTCP19-H* might have been preferably preserved in rice varieties in nitrogen-poor regions during domestication.

OsTCP19-H holds the potential for improving NUE

Asian cultivated rice mainly consists of indica and japonica varieties (accounting for about 90% of global rice production)²⁷ in which *OsTCP19-H* has largely been lost, suggesting that this allele has considerable breeding value for improvements in NUE. We therefore carried out large-scale field trials with the *NIL_OsTCP19-H* line and its corresponding recipient parent Kos under two nitrogen conditions (low nitrogen (50 kg ha^{-1}) and moderate nitrogen (150 kg ha^{-1})) for three successive

years (2017, 2018 and 2019). The field test consistently demonstrated that NIL^{*OsTCP19-H*} plants have more tillers than Kos plants in both low and moderate nitrogen conditions (Fig. 5b, c, Extended Data Fig. 10a, c, d). Apart from a slight increase in 1,000-grain weight as well as a decrease in plant height, no significant difference was found between NIL^{*OsTCP19-H*} and Kos plants in other agronomic traits (Supplementary Table 8). These alterations collectively led to a significant increase in grain yield per plant in the NIL^{*OsTCP19-H*} line (Fig. 5d, Extended Data Fig. 10b, e). Notably, in the NIL^{*OsTCP19-H*} line, the actual yield per plot and NUE were increased by about 20% in low nitrogen and about 30% in moderate nitrogen conditions (Fig. 5e, f, Extended Data Fig. 10f, g). Moreover, *OsTCP19-H* introgression into two elite japonica cultivars (Kongyu131 and Xiushui134) also significantly promoted their tillering under both low and moderate nitrogen conditions (Extended Data Fig. 10h–k), which further indicates that *OsTCP19-H* shows great promise for improvements in the NUE of elite rice cultivars.

Discussion

The soil environment is a key driver of local adaptation in plants²⁸. Nonetheless, the genetic basis of this adaptation is still largely unknown. Here we report that allelic variation in *OsTCP19* contributes to geographical adaptation to local soil nitrogen. Moreover, our findings also hint at different adaptation scenarios to local soil nitrogen conditions. The high allele frequency of *OsTCP19-H* in wild rice suggests that *OsTCP19-H* was subjected to natural selection in natural habitats that usually have a low nitrogen content. During rice domestication in different geographical locations, the nitrogen content in the field soil could be highly varied. In nitrogen-deficient regions *OsTCP19-H* is retained under the selective pressure of low nitrogen, whereas in nitrogen-rich regions *OsTCP19-H* is lost (possibly related to relaxed selection pressure). With the over-application of nitrogen fertilizer, rice would produce too many tillers and consequently raise the risk of unproductive tiller formation and trade-off effects for other agronomic traits, which is a major concern for high-yielding rice breeding^{29–31}—this probably imposes a negative selection on *OsTCP19-H* in modern cultivars. To achieve the current aim of obtaining higher yields with lower nitrogen, it is necessary to bring the lost allele back into modern cultivars.

Our work here also reveals a regulatory cascade of nitrogen-modulated plant development. *OsTCP19* is itself nitrogen-regulated and targets to *DLT*, a vital component in brassinosteroid signalling. The *OsTCP19–DLT* module thus integrates nitrogen and brassinosteroid signalling to transduce an environmental nitrogen stimulus to regulate the developmental process. In addition, *OsTCP19* can also modulate the expression of nitrogen-utilization genes (Extended Data Fig. 10l, m) and *OsTCP19-H* confers a higher nitrogen absorption ability (Extended Data Fig. 10n), which indicates a more integrative role of *OsTCP19* in response to nitrogen. On the one hand, *OsTCP19* mediates the nitrogen-triggered development process by regulating the expression of tillering-promoting genes. On the other hand, *OsTCP19* further tunes nitrogen absorption by regulating the expression of nitrogen-utilization genes to meet the increased nitrogen demand for development. Future work that addresses the integration of the signal pathways of plant development and nitrogen utilization in response to nitrogen nutrition will be key for comprehensively understanding NUE in plants.

Online content

Any methods, additional references, Nature Research reporting summaries, source data, extended data, supplementary information,

acknowledgements, peer review information; details of author contributions and competing interests; and statements of data and code availability are available at <https://doi.org/10.1038/s41586-020-03091-w>.

- Zhang, X. et al. Managing nitrogen for sustainable development. *Nature* **528**, 51–59 (2015).
- Guo, J. H. et al. Significant acidification in major Chinese croplands. *Science* **327**, 1008–1010 (2010).
- Tong, H. et al. DWARF AND LOW-TILLERING, a new member of the GRAS family, plays positive roles in brassinosteroid signaling in rice. *Plant J.* **58**, 803–816 (2009).
- Tong, H. et al. DWARF AND LOW-TILLERING acts as a direct downstream target of a GSK3/SHAGGY-like kinase to mediate brassinosteroid responses in rice. *Plant Cell* **24**, 2562–2577 (2012).
- Hakeem, K. R., Ahmad, A., Iqbal, M., Gucel, S. & Ozturk, M. Nitrogen-efficient rice cultivars can reduce nitrate pollution. *Environ. Sci. Pollut. Res.* **18**, 1184–1193 (2011).
- Wang, F. & Peng, S. Yield potential and nitrogen use efficiency of China's super rice. *J. Integr. Agric.* **16**, 1000–1008 (2017).
- Savolainen, O. The genomic basis of local climatic adaptation. *Science* **334**, 49–50 (2011).
- Russell, J. et al. Exome sequencing of geographically diverse barley landraces and wild relatives gives insights into environmental adaptation. *Nat. Genet.* **48**, 1024–1030 (2016).
- Navarro, J. A. R. et al. A study of allelic diversity underlying flowering-time adaptation in maize landraces. *Nat. Genet.* **49**, 476–480 (2017).
- Hu, B. et al. Variation in *NRT1.1B* contributes to nitrate-use divergence between rice subspecies. *Nat. Genet.* **47**, 834–838 (2015).
- Li, S. et al. Modulating plant growth-metabolism coordination for sustainable agriculture. *Nature* **560**, 595–600 (2018).
- Wu, K. et al. Enhanced sustainable green revolution yield via nitrogen-responsive chromatin modulation in rice. *Science* **367**, eaaz2046 (2020).
- Wang, H. et al. The power of inbreeding: NGS-based GWAS of rice reveals convergent evolution during rice domestication. *Mol. Plant* **9**, 975–985 (2016).
- Xu, G., Fan, X. & Miller, A. J. Plant nitrogen assimilation and use efficiency. *Annu. Rev. Plant Biol.* **63**, 153–182 (2012).
- Mukhopadhyay, P. & Tyagi, A. K. *OsTCP19* influences developmental and abiotic stress signaling by modulating ABI4-mediated pathways. *Sci. Rep.* **5**, 9998 (2015).
- Nicolas, M. & Cubas, P. TCP factors: new kids on the signaling block. *Curr. Opin. Plant Biol.* **33**, 33–41 (2016).
- Rubin, G., Tohge, T., Matsuda, F., Saito, K. & Scheible, W. R. Members of the LBD family of transcription factors repress anthocyanin synthesis and affect additional nitrogen responses in *Arabidopsis*. *Plant Cell* **21**, 3567–3584 (2009).
- Li, C. et al. OsLBD37 and OsLBD38, two class II type LBD proteins, are involved in the regulation of heading date by controlling the expression of *Ehd1* in rice. *Biochem. Biophys. Res. Commun.* **486**, 720–725 (2017).
- Endo, M. et al. CDKB2 is involved in mitosis and DNA damage response in rice. *Plant J.* **69**, 967–977 (2012).
- Hu, Y. & Lai, Y. Identification and expression analysis of rice histone genes. *Plant Physiol. Biochem.* **86**, 55–65 (2015).
- Luo, L. et al. OsASN1 plays a critical role in asparagine-dependent rice development. *Int. J. Mol. Sci.* **20**, 130 (2018).
- Fang, Z. et al. Strigolactones and brassinosteroids antagonistically regulate the stability of the D53-OsBZR1 complex to determine *FC1* expression in rice tillering. *Mol. Plant* **13**, 586–597 (2020).
- Alexandrov, N. et al. SNP-Seek database of SNPs derived from 3000 rice genomes. *Nucleic Acids Res.* **43**, D1023–D1027 (2015).
- Xie, W. et al. Breeding signatures of rice improvement revealed by a genomic variation map from a large germplasm collection. *Proc. Natl. Acad. Sci. USA* **112**, E5411–E5419 (2015).
- Glaszmann, J. C. Isozymes and classification of Asian rice varieties. *Theor. Appl. Genet.* **74**, 21–30 (1987).
- Huang, X. et al. A map of rice genome variation reveals the origin of cultivated rice. *Nature* **490**, 497–501 (2012).
- Muthayya, S., Sugimoto, J. D., Montgomery, S. & Maberly, G. F. An overview of global rice production, supply, trade, and consumption. *Ann. N. Y. Acad. Sci.* **1324**, 7–14 (2014).
- Guerrero, J., Andrello, M., Burgarella, C. & Manel, S. Soil environment is a key driver of adaptation in *Medicago truncatula*: new insights from landscape genomics. *New Phytol.* **219**, 378–390 (2018).
- Khush, G. S. Breaking the yield frontier of rice. *GeoJournal* **35**, 329–332 (1995).
- Yang, W., Peng, S., Laza, R. C., Visperas, R. M. & Dionisiosepe, M. L. Grain yield and yield attributes of new plant type and hybrid rice. *Crop Sci.* **47**, 1393–1400 (2007).
- Peng, S., Khush, G. S., Virk, P. S., Tang, Q. & Zou, Y. Progress in ideotype breeding to increase rice yield potential. *Field Crops Res.* **108**, 32–38 (2008).
- R Core Team. R: A Language and Environment for Statistical Computing, <https://www.R-project.org/> (R Foundation for Statistical Computing, 2017).

Publisher's note Springer Nature remains neutral with regard to jurisdictional claims in published maps and institutional affiliations.

© The Author(s), under exclusive licence to Springer Nature Limited 2020

Article

Methods

No statistical methods were used to predetermine sample size. Phenotyping of agronomic traits and samplings of plant tissues were performed via randomly selecting plants grown under the same conditions or treatments. The investigators were not blinded to allocation during experiments and outcome assessment.

Plant materials

All the 110 accessions of the Mini-Core Collection are listed in Supplementary Table 2. The Mini-Core Collection was requested from USDA-ARS, as previously reported¹³. The japonica rice varieties Zhonghua 11 (ZH11), Koshihikari (Kos), Kongyu131 (KY131) and Xiushu134 (XS134) were used in this study. The T-cr knockout mutants, *OsTCP19*-L gene-edited (TGE) plants and all transgenic lines were generated in the ZH11 background; NIL^{*OsTCP19*-H} was developed by backcrossing with the japonica variety Kos. KY131^{*OsTCP19*-H} and XS134^{*OsTCP19*-H} were developed by backcrossing for five generations with NIL^{*OsTCP19*-H} in the KY131 and XS134 background, respectively. The *dlt* mutant was previously identified³. Primer sequences used for genotyping are listed in Supplementary Table 9.

Hydroponic culture of rice

Hydroponic culture (gene expression detection and rice protoplast preparation) was performed in a growth chamber with 12 h light (28 °C) and 12 h dark (25 °C) photoperiod, about 70% humidity and about 200 μmol m⁻² s⁻¹ photon density. About 200 rice seedlings were cultivated in 750 ml Kimura B nutrient solution (usually as normal nitrogen condition) including macronutrients (0.37 mM (NH₄)₂SO₄, 0.18 mM KNO₃, 0.37 mM Ca(NO₃)₂, 0.18 mM KH₂PO₄, 0.09 mM K₂SO₄, 0.55 mM MgSO₄·7H₂O, 0.16 mM Na₂SiO₃·9H₂O) and micronutrients (46.2 μM H₃BO₃, 0.32 μM CuSO₄·5H₂O, 9.14 μM MnCl₂·4H₂O, 0.08 μM (NH₄)₆Mo₇O₂₄·4H₂O, 0.76 μM ZnSO₄·7H₂O, and 40 μM Fe(II)-EDTA), pH 5.75. The nutrient solution was replaced every day.

For culture with different nitrogen concentrations, (NH₄)₂SO₄ and KNO₃ were replaced by NH₄NO₃, and Ca(NO₃)₂ was replaced by CaCl₂·2H₂O. We used 0.05 mM, 0.15 mM, 0.3 mM, 0.75 mM, 1.25 mM and 2.5 mM NH₄NO₃ for hydroponic culture. In comparison with the nitrogen concentration of Kimura B solution (1.7 mM), 0.15 mM NH₄NO₃ was used as low nitrogen and 1.25 mM NH₄NO₃ was used as moderate nitrogen in this study. For nitrate or ammonium treatment, KNO₃ or NH₄Cl were used as the sole nitrogen source and Ca(NO₃)₂ was replaced by CaCl₂·2H₂O.

Rice cultivation conditions

Rice Mini-Core Collection was grown during the cultivation season (July to November) in 2015 at the experimental station of the South China Agricultural University in Guangzhou. Rice seeds were sown on the seed bed in July and grown for 30 days, then the seedlings were transplanted to the field and left until the harvest stage in November. For each accession, the plant spacing was 20 cm, and 8 plants × 3 rows were planted under low, moderate and high nitrogen conditions.

Large-scale field tests of Kos, NIL^{*OsTCP19*-H}, ZH11 and cTO lines were performed at the experimental station of the Institute of Genetics and Developmental Biology (IGDB) in Beijing for three years (2017 to 2019). At the beginning of May, rice seeds were sown on the seed bed for a one-month growth. Next, rice seedlings were transplanted to the field and left until the harvest stage in October. The plant spacing was 20 cm, and 8 plants × 10 rows were transplanted to each plot. Four replicates were set for plot yield tests under low and moderate nitrogen conditions.

The field tests of low-TRN varieties, high-TRN varieties, KY131, KY131^{*OsTCP19*-H}, XS134 and XS134^{*OsTCP19*-H} were performed at the experimental station of the IGDB in Lingshui. Thirty-day-old rice seedlings from the seed bed were transplanted to the field at the beginning of

November; after two months of growth, tiller number was analysed in the harvest stage. For each line, 8 plants × 8 rows with 20-cm spacing were grown under low and moderate nitrogen conditions. For the field trials in Beijing, Guangzhou and Lingshui, urea was used as the nitrogen source and kg of net nitrogen was applied per ha. Fifty kg per ha was applied for the low nitrogen condition, 150 kg ha⁻¹ for the moderate nitrogen condition and 300 kg ha⁻¹ for the high nitrogen condition. The nitrogen was applied at three stages: the seedling stage, tillering stage and heading stage. The NUE was defined as the grain yield per unit of available nitrogen in the soil³³.

Seeds of ZH11 and TGE plants were sown on the seed bed at the beginning of May for 30 days and then transplanted to a greenhouse under natural light at 30 °C (day) and 25 °C (night) and cultivated for one month in 2020. Each seedling was grown in one plastic pot (8 cm × 8 cm × 8 cm) and urea was used as the nitrogen source with net nitrogen 0.5 kg m⁻² for low nitrogen and 1.5 kg m⁻² for moderate nitrogen.

GWA mapping

Agronomic traits of Rice Mini-Core Collection including tiller number, grain number per panicle and 1,000-grain weight were surveyed at rice harvest stage (about 120 days after germination (November 2015)) under 3 nitrogen conditions. The nitrogen response value was obtained according to the increased value from low to moderate nitrogen relative to the value of low nitrogen ((moderate nitrogen – low nitrogen)/low nitrogen). Subsequently, TRN—the highest variable value response to nitrogen—was used for GWAS.

For GWAS, we used the previously reported SNP dataset¹³. We filtered SNPs with minor allele frequency (MAF) lower than 5% for the 110 rice accessions with phenotypes, retaining 1,889,946 SNPs for the analysis. The analysis was performed using GEMMA (version 0.941) by fitting a linear mixed model³⁴, and we also included first four principal components from the principal component analysis (PCA) as covariates to control for population structure. The threshold for genome-wide significance was determined by Bonferroni correction (that is, corrected $P=0.05/n$, in which n is the number of independent SNPs across the genome). The n was estimated by pruning the SNP dataset using PLINK (version 1.9) with arguments ‘1000kb 10kb 0.2’³⁵, retaining 19,881 independent SNPs. The genome-wide significance level for TRN was determined as 2.5×10^{-6} . For association analysis of *OsTCP19* PCR amplification data with TRN, a total of 35 variants (v1–v35) were generated and variants with MAF ≥ 5% were retained for further analysis. Seven variants (v3, v6, v8, v13, v20, v24 and v26) significantly associated with TRN were finally identified. The information of the variants is listed in Supplementary Table 2.

PCA analysis

The PCA was performed using ngsCovar³⁶ from ngsTools³⁷ software package. The method is based on genotype likelihoods, which accounts for uncertainty and sequencing errors and is suitable for low-coverage data. The full SNP dataset was first thinned by randomly picking 1 SNP in every 5-kb region, yielding 62,606 sites. The genotype likelihoods at these sites were called using ANGSD (version 0.931)³⁸ with ‘-doGL 2-GL1’³⁹ arguments.

Constructs for genetic transformation

An approximately 3.8-kb DNA fragment of *OsTCP19* containing 2,240-bp upstream sequence, *OsTCP19* coding sequence and 440-bp downstream sequence was amplified from ZH11 and cloned into pCAMBIA2300 to generate pCAMBIA2300-pro*OsTCP19*:*OsTCP19* overexpression construct. For the *OsTCP19* RNA-interference vector, *OsTCP19*-specific sequence across the coding region and 3' untranslated region was amplified, and the sense and antisense orientation were inserted into a modified pCAMBIA2300-RNAi vector. The full-length coding sequence of *OsTCP19* from ZH11 was inserted into pCAMBIA2300 vector to generate pCAMBIA2300-35S:*OsTCP19* constructs.

The full-length coding sequences of *OsTCP19* from Kos and Kasa were cloned into pCAMBIA1300-35S-Flag vector to generate pCAMBIA1300-35S:OsTCP19-L-Flag and pCAMBIA1300-35S:OsTCP19-H-Flag constructs. For the *DLT*-overexpression vector, a 5.7-kb genomic fragment of *DLT* containing the promoter and coding regions was amplified from ZH11 and then inserted into pCAMBIA1300. Two small-guide RNA sequences from the *OsTCP19* coding region were cloned into pYLCRISPR/Cas9-MH vector to generate the *OsTCP19* CRISPR-Cas9 construct. One small-guide RNA sequence from the 29-bp indel was designed and inserted into pYLCRISPR/Cas9-MH vector to generate *OsTCP19* genome-editing constructs. Full-length coding sequences of *OsLBD37* and *OsLBD39* were amplified from ZH11 and inserted into pCAMBIA2300 to generate pCAMBIA2300-35S:OsLBD37 and pCAMBIA2300-35S:OsLBD39 constructs. An approximately 2.6-kb genomic region of *OsLBD37* and a 3.4-kb genomic region of *OsLBD39* were cloned into pCAMBIA1300 to generate pCAMBIA1300-proOsLBD37:OsLBD37 and pCAMBIA1300-proOsLBD39:OsLBD39 overexpression constructs, respectively. *Agrobacterium*-mediated transformation was used to generate transgenic rice plants. Primer sequences used in this study are listed in Supplementary Table 9.

RNA isolation and qRT-PCR

Total RNA was extracted using TRIzol reagent (Invitrogen) and the RNA was reversely transcribed using ReverTra Ace qPCR RT Master Mix (Toyobo) according to the manufacturer's instructions. qPCR was performed using SYBR Green Real-Time PCR Master Mix (Toyobo) according to manufacturer's protocol, and three independent RNA samples were prepared for biological replicates. The rice *ACTIN1* gene was used as the internal reference and the relevant primers for qPCR are listed in Supplementary Table 9.

RNA-sequencing analysis

Roots of two-week-old rice seedlings grown in hydroponic culture were used for total RNA isolation. For each line, roots of 48 seedlings were collected for sampling. RNA-sequencing libraries were prepared from ZH11 and *OsTCP19*-overexpression lines with three replicates. The libraries were sequenced using BGISEQ-500 platform and the generated reads were cleaned and then mapped to the reference genome. After normalization, the generated FPKM value was used to analyse the transcript abundance. DEG identification was performed with a threshold of *Q* value < 0.001 and absolute value of fold change > 1.5 in TO1 and TO2 lines versus ZH11. For TCP-binding *cis*-element screening, 1.3-kb sequence including +1 kb and -0.3 kb relative to the transcription start site of the 822 DEGs mentioned in 'OsTCP19-DLT module underlies TRN regulation' were extracted, and AtTCP14 and AtTCP15 binding sites were predicted according to <http://meme-suite.org/doc/download.html>, with *P* < 0.0001. For the nitrogen-responsive gene-set definition, genes with a continuously upregulated or downregulated expression pattern that is similar to that of *OsTCP19* from 0 mM, 2 mM and 10 mM nitrate conditions were selected, with *P* < 0.05 and absolute value of fold change > 1.

Subcellular localization assay

To detect the subcellular localization of OsTCP19, full-length cDNAs of *OsTCP19* from ZH11 and Kasa were amplified and inserted into pCAMBIA2300-35S:eGFP vector. The resulting constructs were purified and then transformed into rice protoplasts. The fluorescence signals were captured by a confocal laser-scanning microscope (TCS SP5; Leica). Primers used for amplification are shown in Supplementary Table 9.

Luciferase activity assay in rice protoplasts

For analysis of the *OsTCP19* promoter in response to nitrogen, approximately 2.2-kb DNA fragments upstream of *OsTCP19* coding region were amplified from Kos and Kasa and inserted into pGreenII 0800-LUC vector to generate proOsTCP19-L:LUC and

proOsTCP19-H:LUC, respectively. Five variants were mutated on the basis of proOsTCP19-L:LUC using Q5 site-directed mutagenesis kit (NEB, E0552S) according to the manufacturer's protocol. The primers used for PCR amplification and mutation are listed in Supplementary Table 9. Ten-day-old rice seedlings grown in low nitrogen nutrient solution (0.1 mM NH₄NO₃) were prepared for protoplasts. All the vectors were transformed into protoplasts, and each transformation product was divided into two portions, adding 0.75 mM and 10 mM NH₄NO₃ to the transformation products to generate low-nitrogen and high-nitrogen conditions, respectively. Afterwards, all the products were incubated in W5 solution for 4–6 h at 28 °C. Activities of firefly luciferase (LUC) and *Renilla* luciferase (REN) were examined using a Dual-Luciferase Reporter Assay System kit (Promega, E1960). LUC/REN was calculated as the relative activity and the ratio of (low nitrogen – high nitrogen)/high nitrogen was used to indicate nitrogen response. For each vector, five replicates were used to evaluate the nitrogen response.

For analysing the transcriptional repression activity of LBD proteins to *OsTCP19*, two effectors (35S-*OsLBD37* and 35S-*OsLBD39*) were cotransformed with reporters (proOsTCP19-L:LUC, proOsTCP19-L v3m:LUC and proOsTCP19-H:LUC) into rice protoplasts. After 12 h incubation at 28 °C, activities of LUC and REN were tested and LUC/REN was used to evaluate the effect of LBD on *OsTCP19*. For *DLT*_{promoter}-LUC activity assay, 35S-*OsTCP19*-L or 35S-*OsTCP19*-H were cotransformed with *DLT*_{promoter}-LUC into rice protoplasts and LUC activities were tested after a 12 h incubation at 28 °C. The related primers are listed in Supplementary Table 9.

ChIP-qPCR assay

The transgenic lines of 35S:*OsTCP19*-L-Flag and 35S:*OsTCP19*-H-Flag cultivated for 2 weeks under moderate nitrogen (1.25 mM NH₄NO₃) condition were used for the ChIP assay. In brief, after being ground in liquid nitrogen, about 1 g materials were crosslinked with 1% formaldehyde for 5 min. The crosslink was stopped with the addition of 0.125 M glycine for 5 min. The chromatin was isolated and sonicated to produce DNA fragments with a size of around 500 bp. Immunoprecipitation was carried out with protein A/G-agarose beads (GE Healthcare, 17152104010150) conjugated to 4 µg of anti-Flag antibody (Sigma, F1804, 1:300 dilution) overnight at 4 °C. Chromatin immunoprecipitated without antibody was used as a control. The precipitated DNA was recovered and analysed by qPCR using the primers listed in Supplementary Table 9.

EMSA

Full-lengths of *OsTCP19*-L and *OsTCP19*-H were amplified and cloned into the pMAL-C2X vector. MBP-OsTCP19-L and MBP-OsTCP19-H recombinant proteins were expressed in the *Escherichia coli* BL21 (DE3) strain and then purified using amylose resin (NEB, E8021S). DNA probes were synthesized and labelled using the Biotin 3' End DNA Labelling Kit (Thermo Fisher Scientific, 89818). The EMSA was performed using the LightShift Chemiluminescent EMSA kit (Thermo Fisher Scientific, 20148). The probe sequences are shown in Supplementary Table 9.

Histological analysis

About 1.5 cm of the shoot base of rice seedlings at four-leaf stage were collected and fixed in FAA (formalin/acetic acid/ethanol) solution at 4 °C overnight. After dehydration and infiltration, all the tissues were embedded in paraffin and then sliced into 8-µm sections (Leica RM2145). The sections were affixed to microscope slides, paraffin was removed and sections were stained with Safranin O and Fast Green for further observation (Leica DMR) and image collection (Apogee Instruments).

Exogenous brassinolide treatment

Fifteen-day-old rice seedlings from field were collected, washed and transplanted to a plastic box containing 12 l Kimura solution with 1 µM brassinolide (WAKO) or an equal volume of DMSO (Sigma).

Article

The seedlings were grown in a greenhouse under natural light at 30 °C (day) and 25 °C (night), and the nutrient solution was changed every 3 days. After 15 days of treatment, the tiller numbers of the seedlings were counted for statistical analysis.

¹⁵N accumulation assay

Rice seedlings were grown in modified Kimura B solution (1.25 mM NH₄NO₃ as the sole nitrogen source) for 10 days. The solutions were changed once a day. Then, the seedlings were pretreated with modified Kimura B solution (1.25 mM NH₄NO₃) was replaced by 1.25 mM NH₄Cl and KNO₃) for 3 h and transferred to a modified Kimura B solution containing 1.25 mM ¹⁵N-NH₄Cl or ¹⁵N-KNO₃ for ¹⁵N-labelling for 3 h. Then, roots of the seedlings were collected after washed with 0.1 mM CaSO₄ solution and deionized water. The samples were dried at 70 °C and then ground to fine powder for ¹⁵N-content detection by an isotope ratio mass spectrometer with an elemental analyser (Thermo Finnigan Delta Plus XP; Flash EA 1112).

Yeast one-hybrid assay

Yeast one-hybrid assay was performed as the following steps. In brief, the promoter region of *DLT* was amplified and inserted into pLacZi2μ vector to generate the *DLT*_{promoter}-*LacZ* reporter construct. The full length of the *OsTCP19* coding sequence was amplified from Kos and Kasa, and then inserted into pJG4-5 vector to generate AD-OsTCP19-L and AD-OsTCP19-H, respectively. AD-OsTCP19-L and AD-OsTCP19-H were then transformed into the yeast strain EGY48 with *DLT*_{promoter}-*LacZ* separately. Transformants were grown on drop-out plates with X-Gal (5-bromo-4-chloro-3-indolyl-β-D-galactopyranoside) for blue colour development according to the instructions (Clontech). Primers are listed in Supplementary Table 9.

Lamina inclination assay

Lamina inclination assay was performed as previously described⁴. Rice seedlings were grown in hydroponic culture for three days after germination. Brassinolide stock solution (20 mM, 10 µg µl⁻¹) was diluted into different concentrations (1,000, 100, 10 and 0 ng µl⁻¹) with ethanol. Then, 1 µl diluted solution was spotted onto the adaxial side of the leaf blade tip. After a three-day incubation, images were taken and the angles of lamina inclination were measured using ImageJ software.

Haplotype analysis of *OsTCP19* promoter in 3K Rice population

The SNPs in the 2.5-kb promoter region of *OsTCP19* of 3,024 varieties were downloaded from Rice SNP-Seek Database (<https://snp-seek.irri.org/>)⁴⁰. The initial dataset has a missing rate of 1.9%, which was imputed using beagle (version 3.3.2)⁴¹. The 151 SNPs were then filtered by applying a MAF ≥ 1% cut-off, retaining 79 high-quality SNPs that define 174 unique haplotypes. Low-frequency haplotypes could arise owing to errors in genotypes calling; we therefore filtered the haplotypes by retaining the ones with frequency ≥ 10, resulting in 20 high-confidence haplotypes.

Allelic variation analysis of *OsTCP19* in wild rice

For allelic variation analysis of *OsTCP19*, an SNP dataset of 446 accessions of common wild rice (*O. rufipogon*) was obtained from a previous study⁴². Five SNPs (chromosome 6: 6569709, 6569967, 6570260, 6570900 and 6571348) tightly linked to the 29-bp insertion were used to access haplotypes of *OsTCP19*. Wild rice accessions with a more than 80% missing data rate (11 accessions) were not used in this study.

Geographical distribution of rice varieties and soil nitrogen content analysis

For geographical distribution of rice varieties from the 3K Rice Genomes Project, six rice subgroups (japonica, indica I, indica II, indica III, aromatic and aus) of the 3,000 varieties were projected to the

map according to their genetic structure and origin information from <http://ricevarmap.ncgr.cn/>⁴⁴. For Pearson correlation coefficient analysis of *OsTCP19*-H allele frequency with soil nitrogen content, 1,764 indica varieties with confirmed location information were selected from 3K Rice Genomes Project, and the *OsTCP19*-H allele frequency was calculated for different countries or regions with more than three indica varieties.

For the analysis of soil nitrogen content of the rice-planting area from 42 countries or regions, we aggregated 5-arc-minute maps of soil nitrogen content into country-scale and vertical-lumped data using area-and depth-weighted methods to match the spatial scale of *OsTCP19*-H allele frequency. First, soil nitrogen content data were collected from a comprehensive global soil dataset at the spatial resolution of 5' × 5'. Soil nitrogen content was averaged by weighting depth from four soil layers (0–4.5 cm, 4.5–9.1 cm, 9.1–16.6 cm and 16.6–28.9 cm) to represent the average level within the root zone. Then, rice-planting area (km² in each grid cell) in recent decades was obtained directly from the History Database of the Global Environment (HYDE 3.2.1) with a spatial resolution identical with the global soil dataset. Area-weighted soil nitrogen content across all of the rice-planting area within a country was acquired to avoid a biased estimation for countries with a small rice-planting area. Climate data, including mean annual temperature and precipitation (1990 to 2014), were collected from the Climatic Research Unit (CRUTS v.3.23). These climate data were extracted over rice-planting area and then averaged into the national-scale values of 42 countries or regions.

Reporting summary

Further information on research design is available in the Nature Research Reporting Summary linked to this paper.

Data availability

The genomic information of Rice Mini-Core Collection has previously been released¹³; the raw sequencing dataset is available on NCBI BioProject (<https://www.ncbi.nlm.nih.gov/bioproject>) under the accession number PRJNA301661. The RNA-sequencing data have been deposited in NCBI's Gene Expression Omnibus (www.ncbi.nlm.nih.gov/geo/) under accession number GSE161265. Data from the 3K Rice Genomes Project can be downloaded from Rice SNP-Seek Database (<https://snp-seek.irri.org/>). Soil nitrogen content data are available from Global Soil Data set (<http://globalchange.bnu.edu.cn>). The data for the rice-planting area of different countries are from the History Database of the Global Environment (HYDE 3.2.1) (<https://doi.org/10.17026/dans-25g-gez3>). Climate data are available from the Climatic Research Unit (CRUTS v.3.23) (https://crudata.uea.ac.uk/cru/data/hrg/cru_ts_3.23/cruts.1506241137.v3.23/). The base map in Fig. 1a was downloaded from <https://www.R-project.org/>³². The base map in Fig. 5a was downloaded from the ArcGIS Hub (https://hub.arcgis.com/datasets/a21fdb46d23e4ef896f31475217cbb08_1 (2020.11.01)). Uncropped data for gel is provided in Supplementary Fig. 1. Source data are provided with this paper.

33. Moll, R., Kamprath, E. & Jackson, W. Analysis and interpretation of factors which contribute to efficiency of nitrogen utilization. *Agron. J.* **74**, 562–564 (1982).
34. Zhou, X. & Stephens, M. Genome-wide efficient mixed-model analysis for association studies. *Nat. Genet.* **44**, 821–824 (2012).
35. Purcell, S. et al. PLINK: a tool set for whole-genome association and population-based linkage analyses. *Am. J. Hum. Genet.* **81**, 559–575 (2007).
36. Fumagalli, M. et al. Quantifying population genetic differentiation from next-generation sequencing data. *Genetics* **195**, 979–992 (2013).
37. Fumagalli, M., Vieira, F. G., Linderöth, T. & Nielsen, R. ngsTools: methods for population genetics analyses from next-generation sequencing data. *Bioinformatics* **30**, 1486–1487 (2014).
38. Korneliussen, T. S., Albrechtsen, A. & Nielsen, R. ANGSD: analysis of next generation sequencing data. *BMC Bioinformatics* **15**, 356 (2014).
39. Li, H. A statistical framework for SNP calling, mutation discovery, association mapping and population genetical parameter estimation from sequencing data. *Bioinformatics* **27**, 2987–2993 (2011).

40. Wang, W. et al. Genomic variation in 3,010 diverse accessions of Asian cultivated rice. *Nature* **557**, 43–49 (2018).
41. Browning, S. R. & Browning, B. L. Rapid and accurate haplotype phasing and missing-data inference for whole-genome association studies by use of localized haplotype clustering. *Am. J. Hum. Genet.* **81**, 1084–1097 (2007).
42. Wang, H., Vieira, F. G., Crawford, J. E., Chu, C. & Nielsen, R. Asian wild rice is a hybrid swarm with extensive gene flow and feralization from domesticated rice. *Genome Res.* **27**, 1029–1038 (2017).

Acknowledgements The pYLCRISPR/Cas9-MH vector was provided by Y. Liu; the pGreenII 0800-LUC vector was provided by X. Chen; and the pJG4-5 and pLacZ12 μ vectors were provided by R. Lin. This work was supported by the grants from the Strategic Priority Research Programme of the Chinese Academy of Sciences (XDA24020000), the National Natural Sciences Foundation of China (31922007), National Key Research and Development of China (2020YFE0202300) and the Major Programme of Guangdong Basic and Applied Research (2019B030302006).

Author contributions Y. Liu performed experiments, analysed the data and wrote the manuscript. H.W. performed the GWA mapping and population genetic analysis. R.X. and H.L. performed the field tests of 110 Mini-Core accessions in Guangzhou. Q.W. and F.Z. collected and analysed the soil nitrogen data. Z.J., W.W., Z.Z., A.L., Y. Liang, S.O., X.L., S.C., H.T. and Y.W. conducted some of the experiments. B.H. and C.C. designed research, wrote the manuscript and supervised the project.

Competing interests The authors declare no competing interests.

Additional information

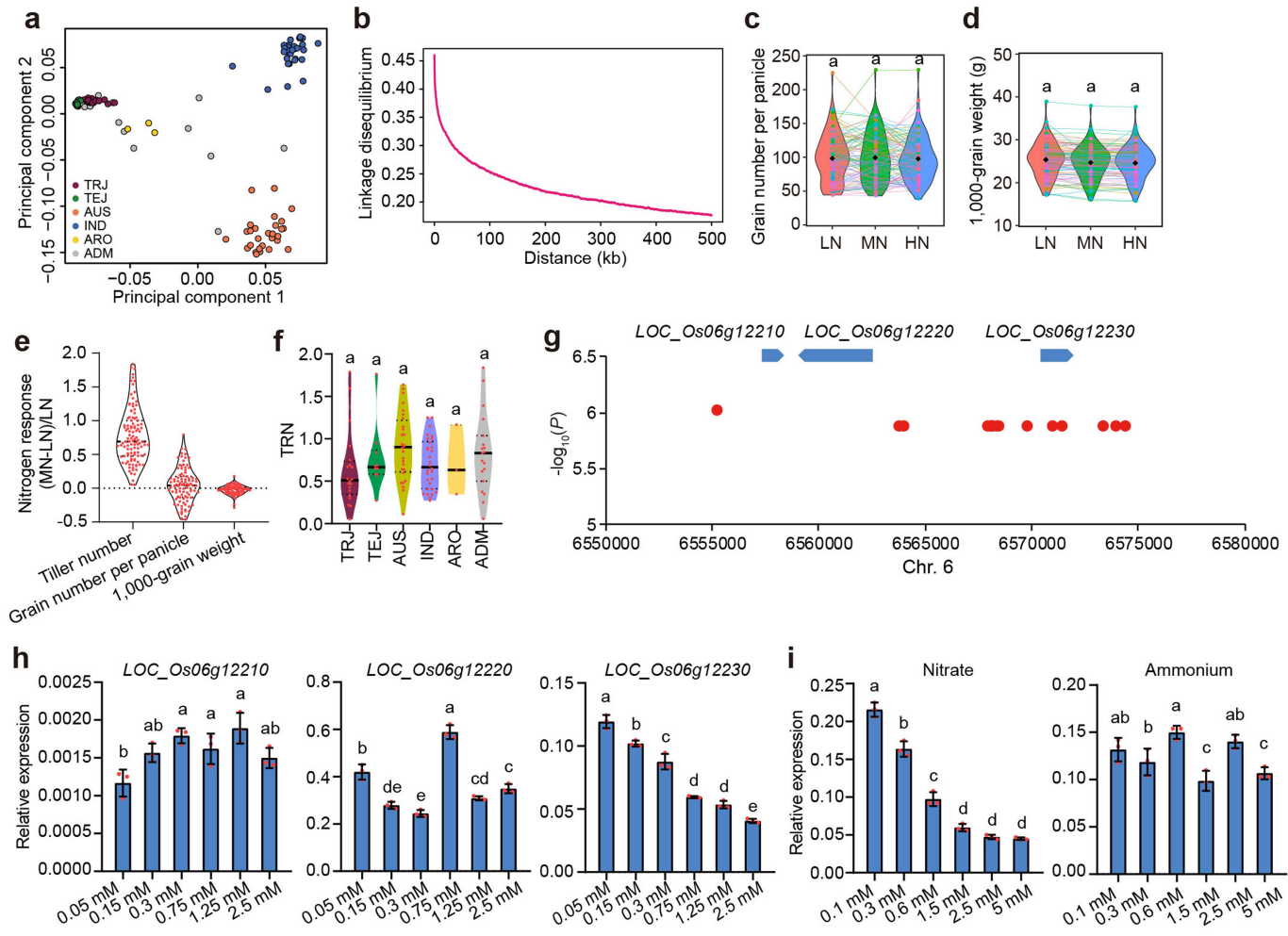
Supplementary information The online version contains supplementary material available at <https://doi.org/10.1038/s41586-020-03091-w>.

Correspondence and requests for materials should be addressed to B.H. or C.C.

Peer review information *Nature* thanks Ando Radanielson, Nicolaus von Wieren and the other, anonymous, reviewer(s) for their contribution to the peer review of this work.

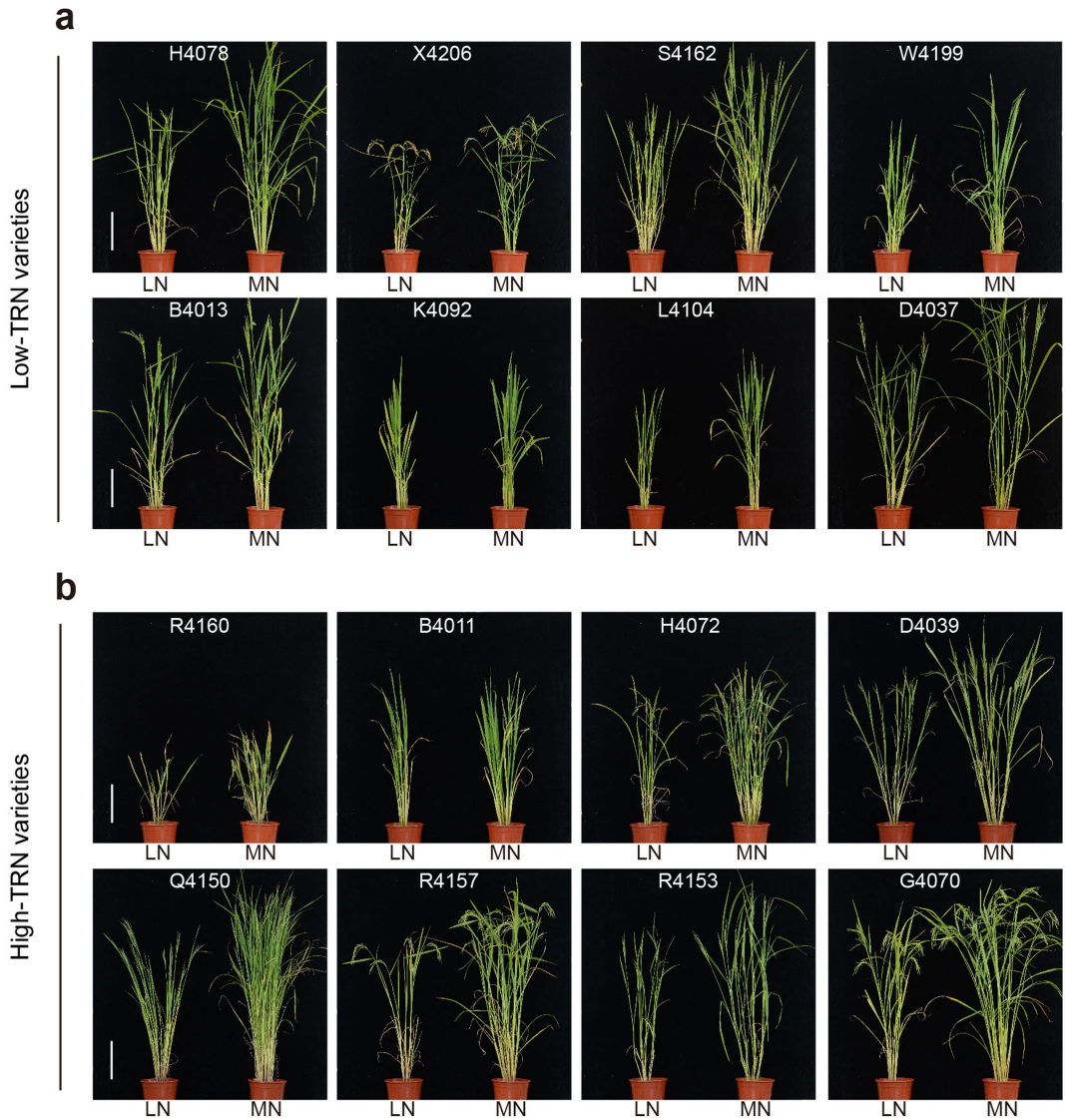
Reprints and permissions information is available at <http://www.nature.com/reprints>.

Article



Extended Data Fig. 1 | Nitrogen response of agronomic traits and expression analysis of three candidate genes. **a**, PCA with genotype likelihoods in 110 accessions. Principal component 1 and principal component 2 divided 110 accessions into 4 groups: japonica, indica, aus and aromatic. **b**, Genome-wide linkage disequilibrium analysis of 110 Mini-Core accessions. **c, d**, Grain number per panicle (**c**) and 1,000-grain weight (**d**) of 110 accessions under low, moderate and high nitrogen conditions in the field. Dots represent individual data points of 110 accessions and lines connect the data points of the same accession under low, moderate and high nitrogen. Black diamonds represent means. For each individual data point, data are average ($n=5$ plants). **e**, Nitrogen response of tiller number, grain number per panicle, and 1,000-grain weight from low to moderate nitrogen. **f**, TRN among different

subgroups. **g**, The position of three candidate genes and the 15 most-significant SNPs that underlie the significant locus on rice chromosome 6. **x** axis, position; **y** axis, P value of the SNPs. Red dots, 15 SNPs. **h**, Expression analysis of three candidate genes by qRT-PCR in the roots of ZH11 plants grown in different nitrogen concentrations (NH_4NO_3). Data are mean \pm s.d. ($n=3$ biologically independent samples). **i**, Expression analysis of *OsTCP19* under different nitrate and ammonium concentrations. Data are mean \pm s.d. ($n=3$ biologically independent samples). **e, f**, The bars in the violin plots represent 25th percentiles, medians and 75th percentiles. In **c, d, f, h, i**, letters indicate significant differences ($P < 0.05$, one-way ANOVA, Tukey's HSD test). For P values, see Source Data.

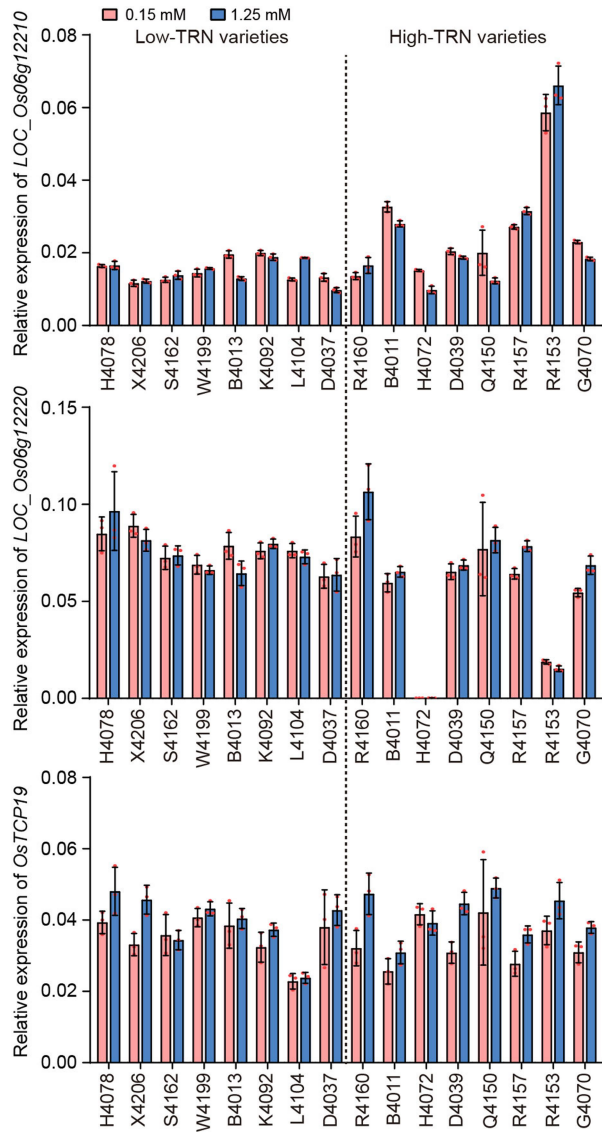


Extended Data Fig. 2 | Phenotype of low-TRN and high-TRN varieties.

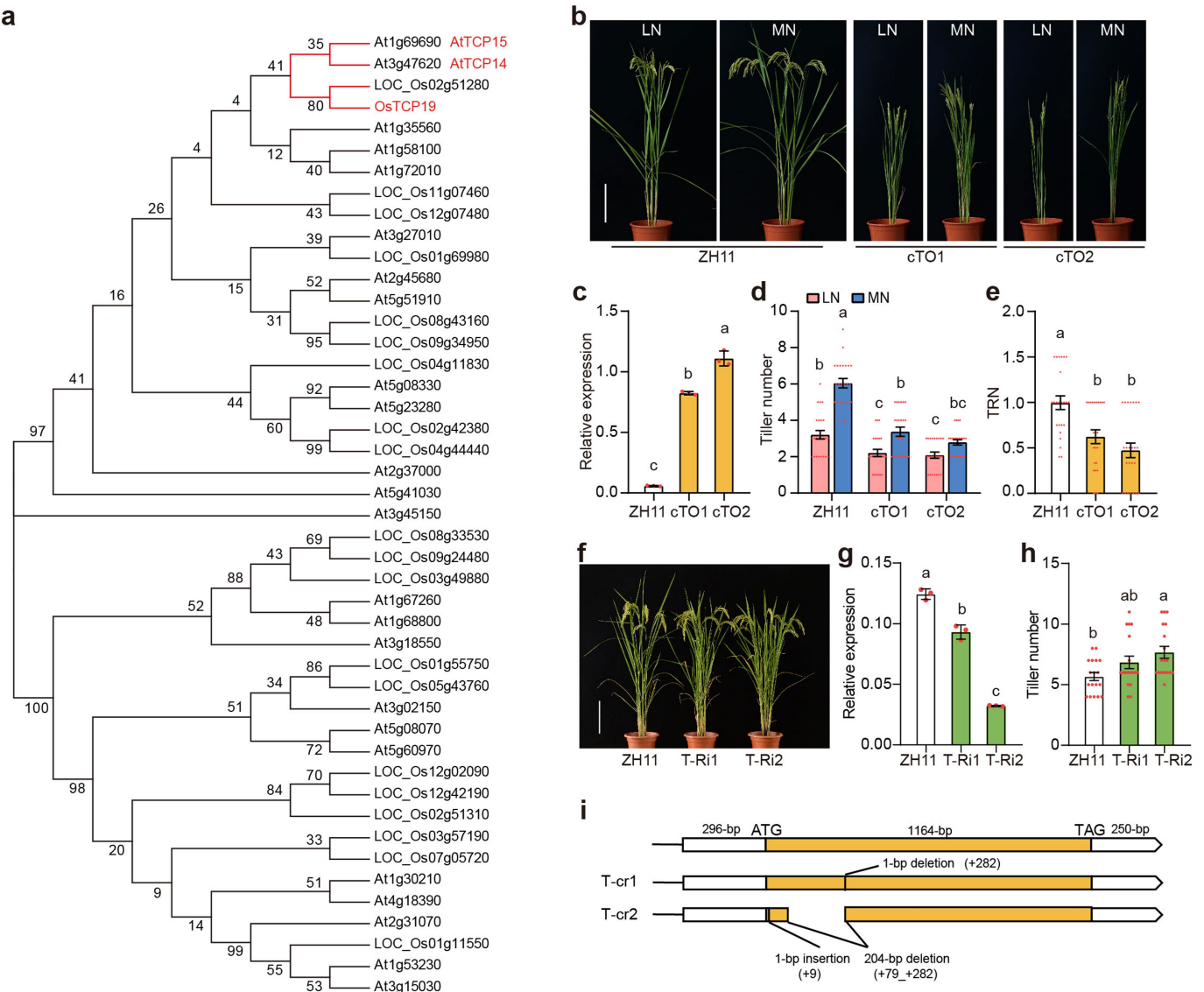
a, b, Phenotype of 8 low-TRN varieties (**a**) and 8 high-TRN varieties (**b**) grown in low nitrogen (50 kg ha^{-1}) and moderate nitrogen (150 kg ha^{-1}) field conditions.

Low-TRN varieties are H4078, X4206, S4162, W4199, B4013, K4092, L4104 and D4037; high-TRN varieties are R4160, B4011, H4072, D4039, Q4150, R4157, R4153 and G4070. Scale bars, 24 cm.

Article



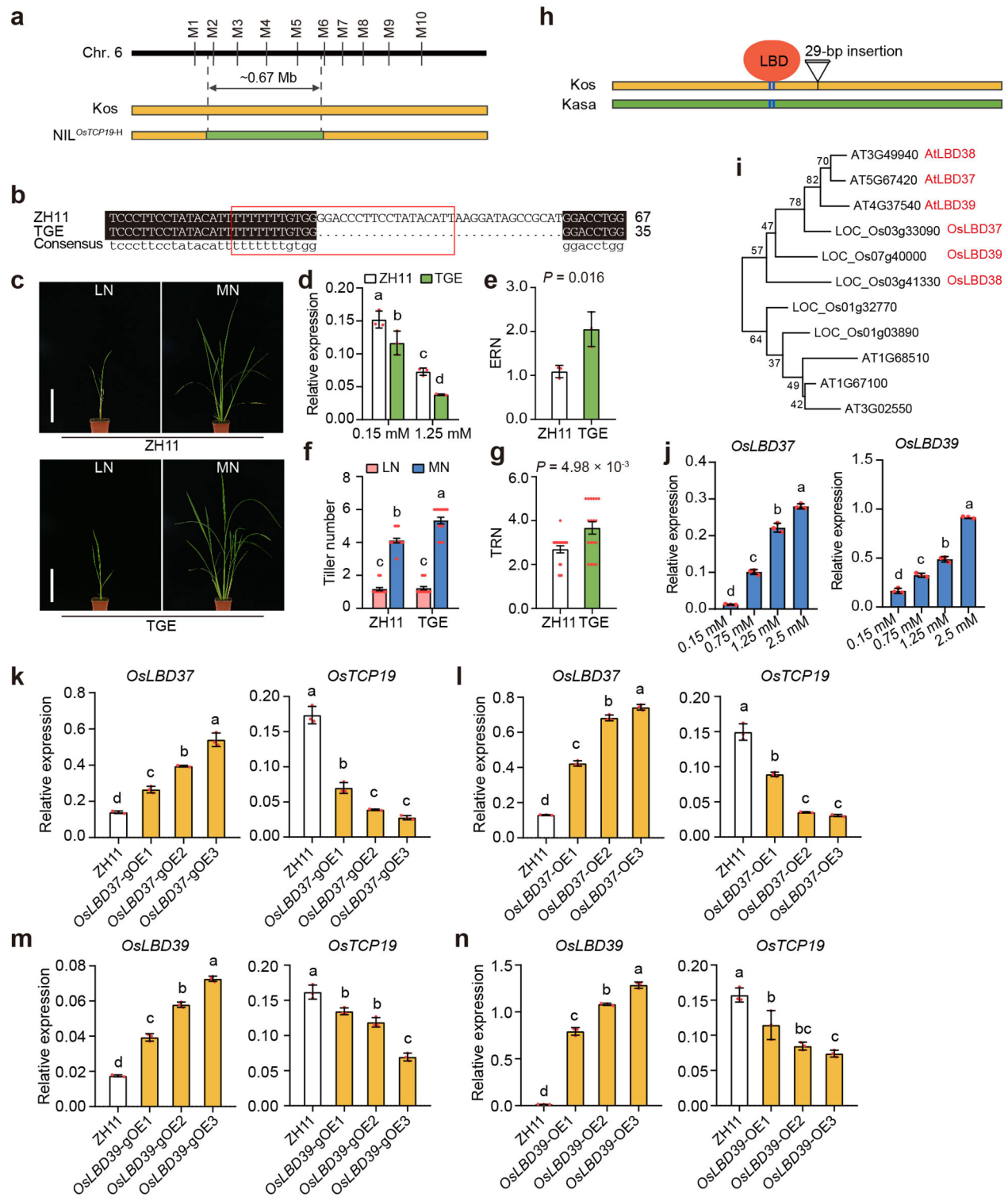
Extended Data Fig. 3 | Transcript expression of three candidate genes in response to nitrogen in the shoot base. Expression analysis of *LOC_Os06g12210*, *LOC_Os06g12220* and *OsTCP19* by qRT-PCR in shoot bases of low-TRN varieties and high-TRN varieties grown in different nitrogen concentrations (NH₄NO₃). Data are mean \pm s.d. ($n = 3$ biologically independent samples).



Extended Data Fig. 4 | OsTCP19 acts as a negative modulator in rice tillering and TRN. **a**, The neighbour-joining tree was constructed in MEGA 5.0. The numbers represent bootstrap (1,000 replicates). OsTCP19 and its orthologues in *Arabidopsis* are shown in red text. **b**, Phenotype of ZH11 and cTO lines (cTO1 and cTO2) under low nitrogen (50 kg ha^{-1}) and moderate nitrogen (150 kg ha^{-1}) conditions. Scale bar, 24 cm. **c**, Expression analysis of *OsTCP19* in ZH11, cTO1 and cTO2 lines by qRT-PCR. Data are mean \pm s.e.m. ($n=3$ biologically independent samples). **d**, Statistical analysis of tiller number per plant of ZH11, cTO1 and cTO2 lines under low and moderate nitrogen conditions. Data are mean \pm s.e.m.

($n=24$ plants). **e**, TRN of ZH11, cTO1 and cTO2 lines generated from **d**. Data are mean \pm s.e.m. ($n=24$ plants). **f**, Phenotype of ZH11, T-Ri1 and T-Ri2. Scale bar, 24 cm. **g**, qRT-PCR analysis of *OsTCP19* expression level in ZH11, T-Ri1 and T-Ri2 lines. Data are mean \pm s.d. ($n=3$ biologically independent samples). **h**, Statistical analysis of tiller number per plant of ZH11, T-Ri1 and T-Ri2 lines. Data are mean \pm s.e.m. ($n=18$ plants). **i**, Diagram of *OsTCP19* CRISPR knockout lines (T-cr1 and T-cr2). The length and the position of the mutations are indicated on the frame. In **c**, **d**, **e**, **g**, **h**, different letters indicate significant differences ($P < 0.05$, one-way ANOVA, Tukey's HSD test). For *P* values, see Source Data.

Article

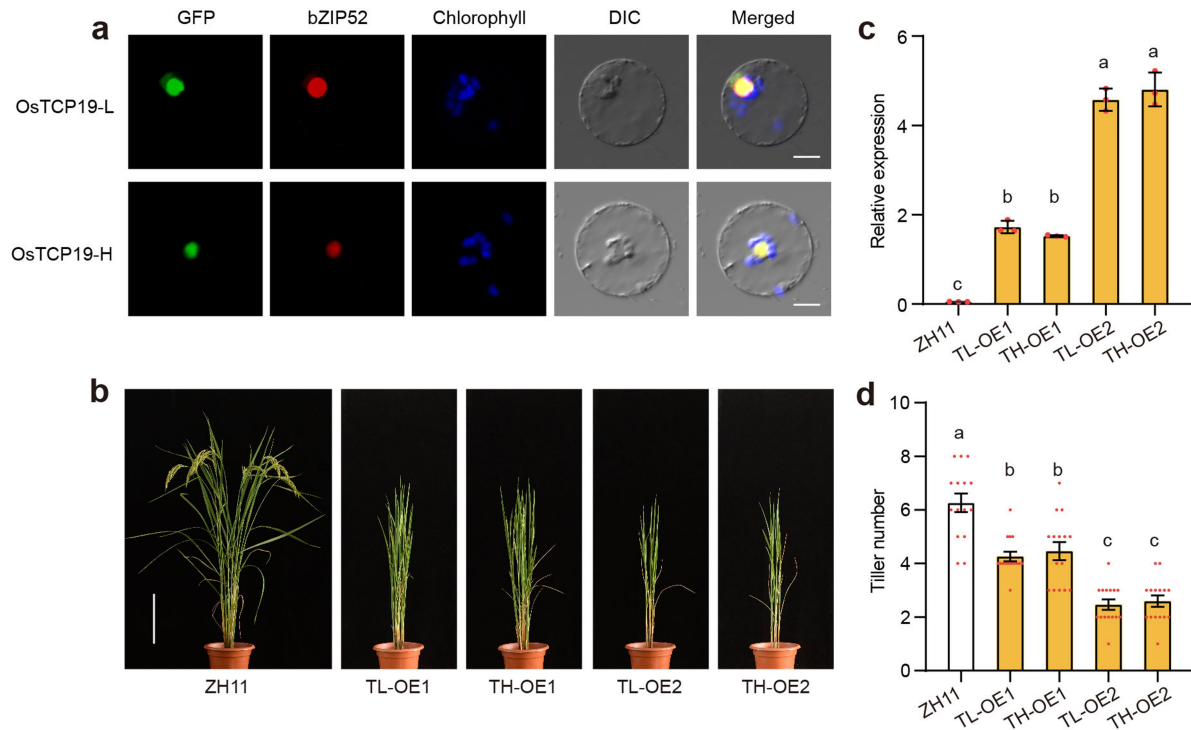


Extended Data Fig. 5 | See next page for caption.

Extended Data Fig. 5 | The 29-bp indel of the *OsTCP19* promoter contributes to TRN variation.

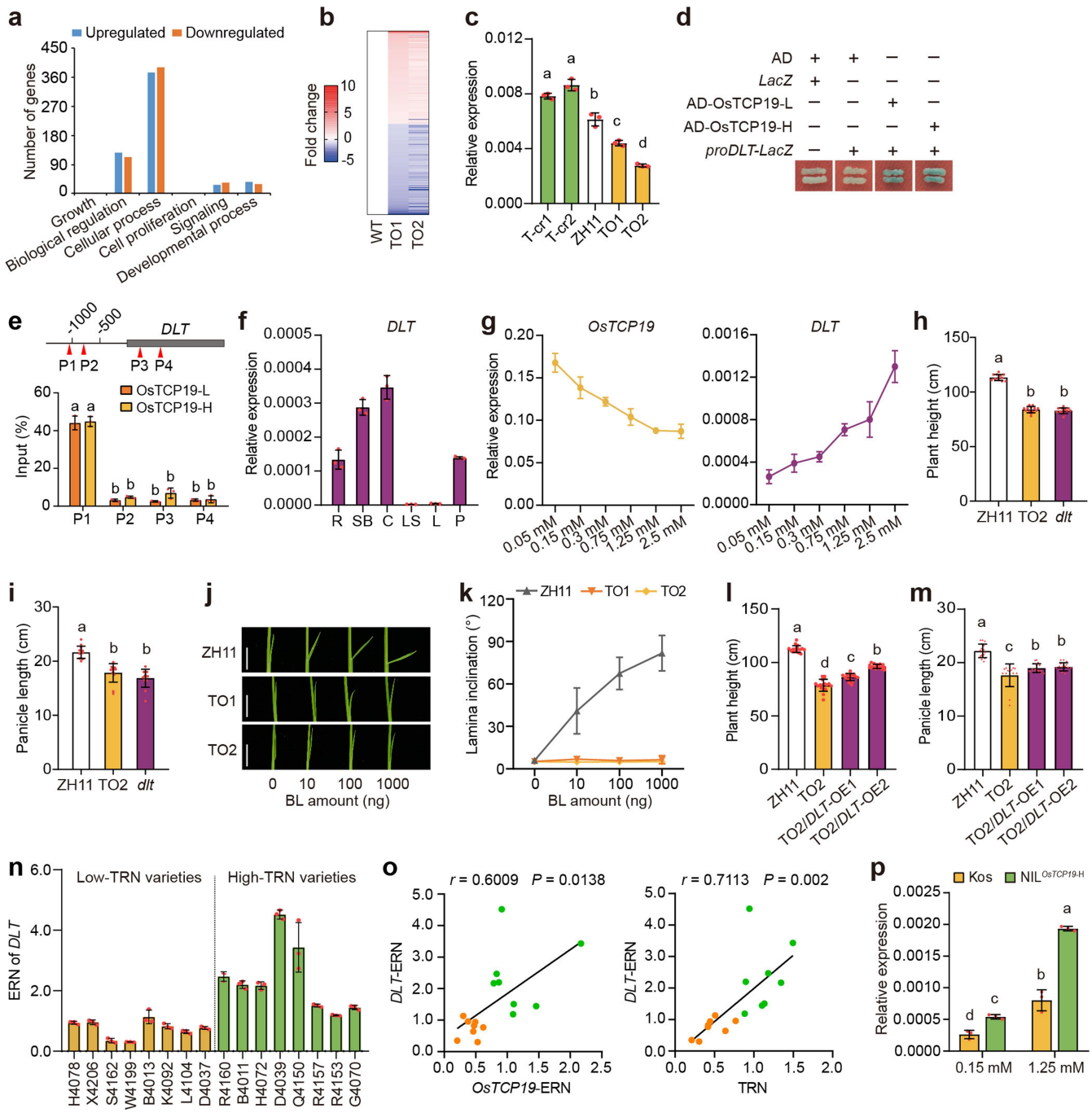
a, Diagram of NIL_{OsTCP19-H}. M1 to M10 represent the molecular markers used for NIL_{OsTCP19-H} construction. Green bar, genomic region from Kasa. The double-headed arrow shows the length of the substitution segment. **b**, Diagram of the *OsTCP19* promoter sequence of ZH11 and TGE line. Red box indicates the position of the 29-bp indel. **c**, Phenotype of ZH11 and TGE plants grown in a greenhouse under low nitrogen (0.5 kg m^{-2}) and moderate nitrogen (1.5 kg m^{-2}) conditions. **d**, qRT–PCR-based transcript abundance analysis of *OsTCP19* in ZH11 and TGE plants grown under 0.15 mM and $1.25 \text{ mM NH}_4\text{NO}_3$. Data are mean \pm s.d. ($n = 3$ biologically independent samples). **e**, ERN of *OsTCP19* generated from **d**. Data are mean \pm s.d. ($n = 3$ biologically independent samples). **f**, Statistical analysis of tiller number per plant of ZH11 and TGE plants of **c**. Data are mean \pm s.e.m. ($n = 18$ plants). **g**, TRN of ZH11 and TGE plants generated from **f**. Data are mean \pm s.e.m. ($n = 18$ plants). **h**, Diagram of the predicted LBD binding sites in *OsTCP19* promoter of Kos and Kasa. Blue bars indicate predicted LBD binding sites. **i**, Phylogenetic analysis of AtLBD37, AtLBD38 and AtLBD39 and their orthologues in rice. The neighbour-joining tree was constructed in MEGA 5.0 and the numbers represent bootstrap of

1,000 replicates. **j**, Expression analysis of *OsLBD37* and *OsLBD39* under different nitrogen (NH_4NO_3) concentrations by qRT–PCR. Data are mean \pm s.d. ($n = 3$ biologically independent samples). **k**, Expression analysis of *OsLBD37* and *OsTCP19* in *OsLBD37* genomic overexpression lines (*OsLBD37-gOE1*, -*gOE2* and -*gOE3*). Data are mean \pm s.d. ($n = 3$ biologically independent samples). **l**, Expression analysis of *OsLBD37* and *OsTCP19* in *OsLBD37* constitutive overexpression lines (*OsLBD37-OE1*, -*OE2* and -*OE3*). Data are mean \pm s.d. ($n = 3$ biologically independent samples). **m**, Expression analysis of *OsLBD39* and *OsTCP19* in *OsLBD39* genomic overexpression lines (*OsLBD39-gOE1*, -*gOE2* and -*gOE3*). Data are mean \pm s.d. ($n = 3$ biologically independent samples). **n**, Expression analysis of *OsLBD39* and *OsTCP19* in *OsLBD39* constitutive overexpression lines (*OsLBD39-OE1*, -*OE2* and -*OE3*). Data are mean \pm s.d. ($n = 3$ biologically independent samples). T_0 generation of *OsLBD37* and *OsLBD39* overexpression lines were used for qRT–PCR analysis and the negative lines were selected as control. In **d**, **f**, **j**–**n**, different letters indicate significant differences at $P < 0.05$ according to one-way ANOVA and Tukey's HSD test. For P values, see Source Data. In **e**, **g**, significant difference was determined by the two-sided Student's *t*-test.



Extended Data Fig. 6 | Two variants of the *OsTCP19* coding region showed no difference in regulating rice tillering. **a**, Subcellular localization of *OsTCP19*-L-GFP and *OsTCP19*-H-GFP fusion proteins in rice protoplasts. Rice transcription factor OsbZIP52 fused with RFP was used as nucleus marker. Scale bars, 10 μ m. **b**, Phenotype of ZH11 and *OsTCP19* overexpression lines driven by the CaMV 35S promoter. TL-OE1 and TL-OE2 represent overexpression lines of *OsTCP19*-L, and TH-OE1 and TH-OE2 represent *OsTCP19*-H overexpression lines.

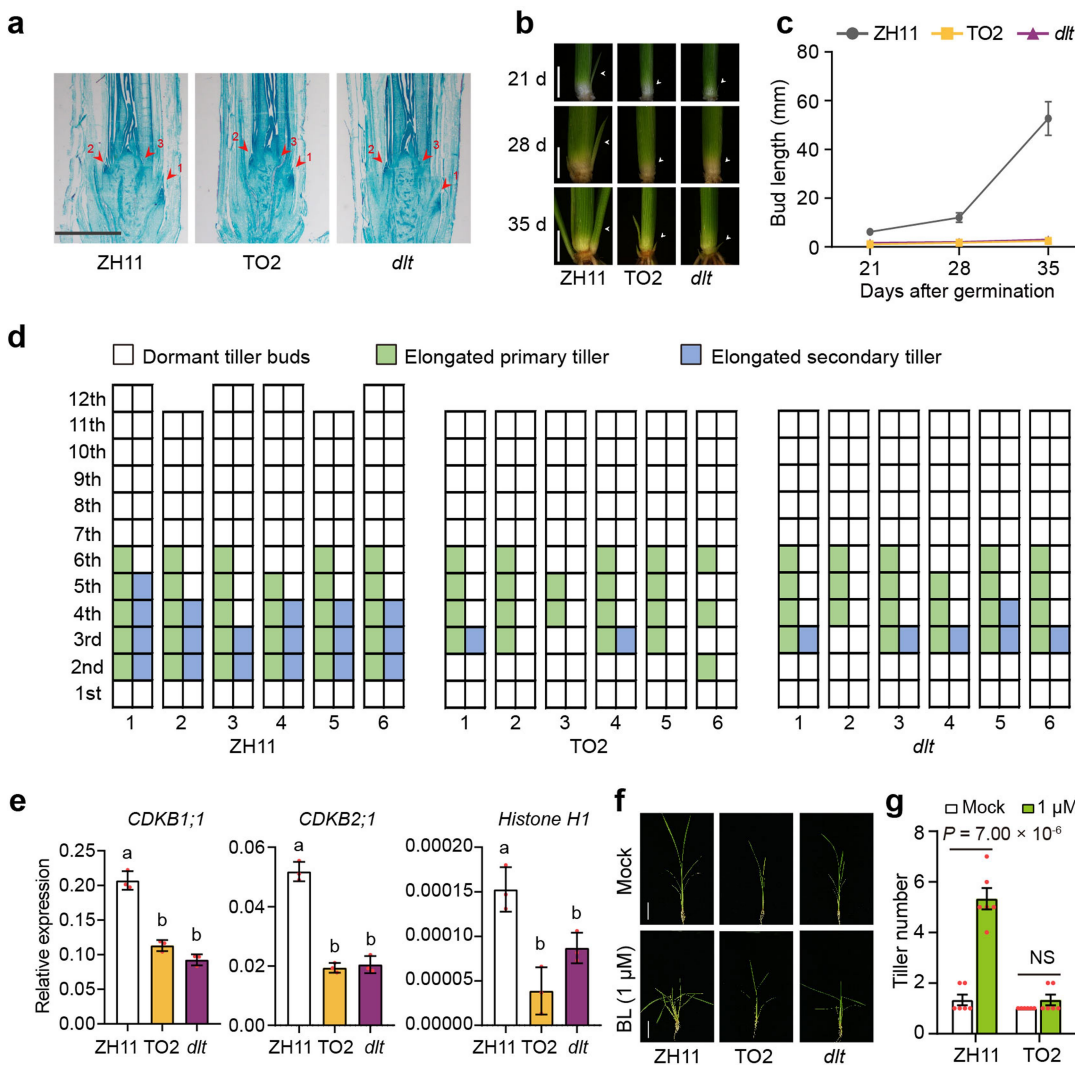
Scale bar, 24 cm. **c**, Expression analysis of *OsTCP19* in ZH11 and *OsTCP19* overexpression lines by qRT-PCR. Data are mean \pm s.d. ($n=3$ biologically independent samples). **d**, Statistical analysis of tiller number per plant of ZH11 and *OsTCP19*-L or *OsTCP19*-H overexpression lines. Data are mean \pm s.e.m. ($n=15$ plants). In **c**, **d**, different letters indicate significant differences at $P<0.05$ according to one-way ANOVA and Tukey's HSD test. For P values, see Source Data.



Extended Data Fig. 7 | DLT was identified as the downstream target of OsTCP19. **a**, Six Gene Ontology (GO) terms were selected by GO analysis. x axis, GO terms; y axis, gene number of each GO term. Blue, upregulated genes; orange, downregulated genes. **b**, A heatmap of 304 TCP-binding DEGs. The colour key (blue to red) represents gene expression (FPKM) as log₂-transformed fold changes of (TO1/WT) or (TO2/WT). **c**, Expression analysis of *DLT* in ZH11, T-cr1, T-cr2 and *OsTCP19*-overexpression lines by qRT-PCR. Data are mean ± s.d. ($n=3$ biologically independent samples). **d**, Binding assays of OsTCP19-L or OsTCP19-H to *DLT* promoter using yeast one-hybrid assay. **e**, Enrichment of OsTCP19-L and OsTCP19-H to the promoter of *DLT* by ChIP-qPCR analysis. The samples were immunoprecipitated with anti-Flag or no antibody (NA) and anti-Flag/NA represents the enrichment fold. Red triangles indicate the position of P1 to P4 on *DLT* genomic sequence. Data are mean ± s.d. ($n=3$ biologically independent samples). **f**, qRT-PCR-based transcript abundance analysis of *DLT* in various tissues. R, roots; SB, shoot bases; C, culms; L, leaves; LS, leaf sheaths; P, panicles. Data are mean ± s.d. ($n=3$ biologically independent samples). **g**, qRT-PCR-based transcript abundance analysis of *OsTCP19* and *DLT* in different nitrogen concentrations (NH_4NO_3). Data are mean ± s.d. ($n=3$ biologically independent samples).

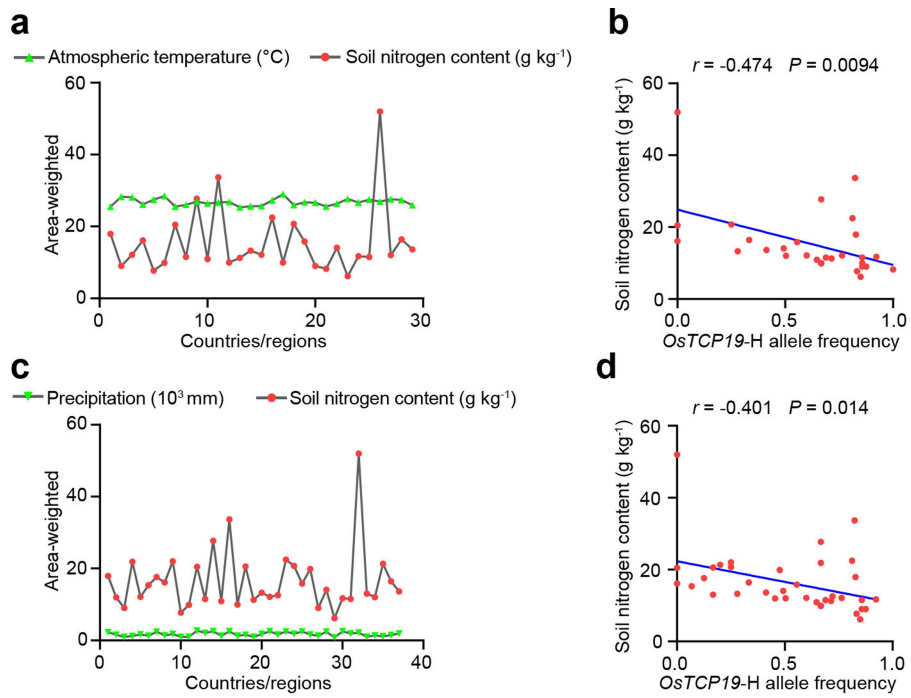
(NH_4NO_3). Data are mean ± s.d. ($n=3$ biologically independent samples). **h, i**, Statistical analysis of plant height (**h**) and panicle length (**i**) of ZH11, TO2 and *dlt* plants. Data are mean ± s.d. ($n=13$ plants). **j**, Brassinosteroid response of ZH11, TO1 and TO2 plants with lamina inclination assay. Scale bars, 1 cm. **k**, Statistical analysis of the lamina inclination in **j**. Data are mean ± s.d. ($n=20$ seedlings). **l, m**, Statistical analysis of plant height (**l**) and panicle length (**m**) of ZH11, TO2, TO2/*DLT*-OE1, and TO2/*DLT*-OE2. Data are mean ± s.d. ($n=17$ plants). **n**, ERN of *DLT* in low-TRN and high-TRN varieties under different nitrogen concentrations (0.15 mM and 1.25 mM NH_4NO_3). Data are mean ± s.d. ($n=3$ biologically independent samples). **o**, Pearson correlation coefficient analysis of ERN of *DLT* with ERN of *OsTCP19* or TRN in low-TRN and high-TRN varieties. Orange, low-TRN varieties; green, high-TRN varieties. **p**, qRT-PCR-based transcript abundance analysis of *DLT* by qRT-PCR in Kos and NIL^{OsTCP19-H} plants under different nitrogen concentrations (NH_4NO_3). Data are mean ± s.d. ($n=3$ biologically independent samples). In **c, e, h, i, l, m, p**, different letters indicate significant differences at $P<0.05$ according to one-way ANOVA and Tukey's HSD test. For *P* values, see Source Data.

Article



Extended Data Fig. 8 | OsTCP19–DLT module modulates rice tillering by regulating tiller bud outgrowth. **a**, Longitudinal sections show no difference in tiller bud initiation in ZH11, TO2 and *dlt* plants. Arrows indicate tiller buds and numbers 1–3 represent the first to third tiller buds. Scale bar, 1 mm. The results are representative of three independent experiments. **b**, Tiller buds in ZH11, TO2 and *dlt* plants at 21, 28 and 35 days after germination. White arrows indicate the third tiller bud (at the axil of the third complete leaf). Scale bars, 0.6 cm. **c**, Statistical analysis of the third tiller bud length of ZH11, TO2 and *dlt* plants. Data are mean \pm s.d. ($n = 5$ seedlings). **d**, Tiller bud outgrowth is repressed in TO2 and *dlt* plants at 90 days after germination. Six independent

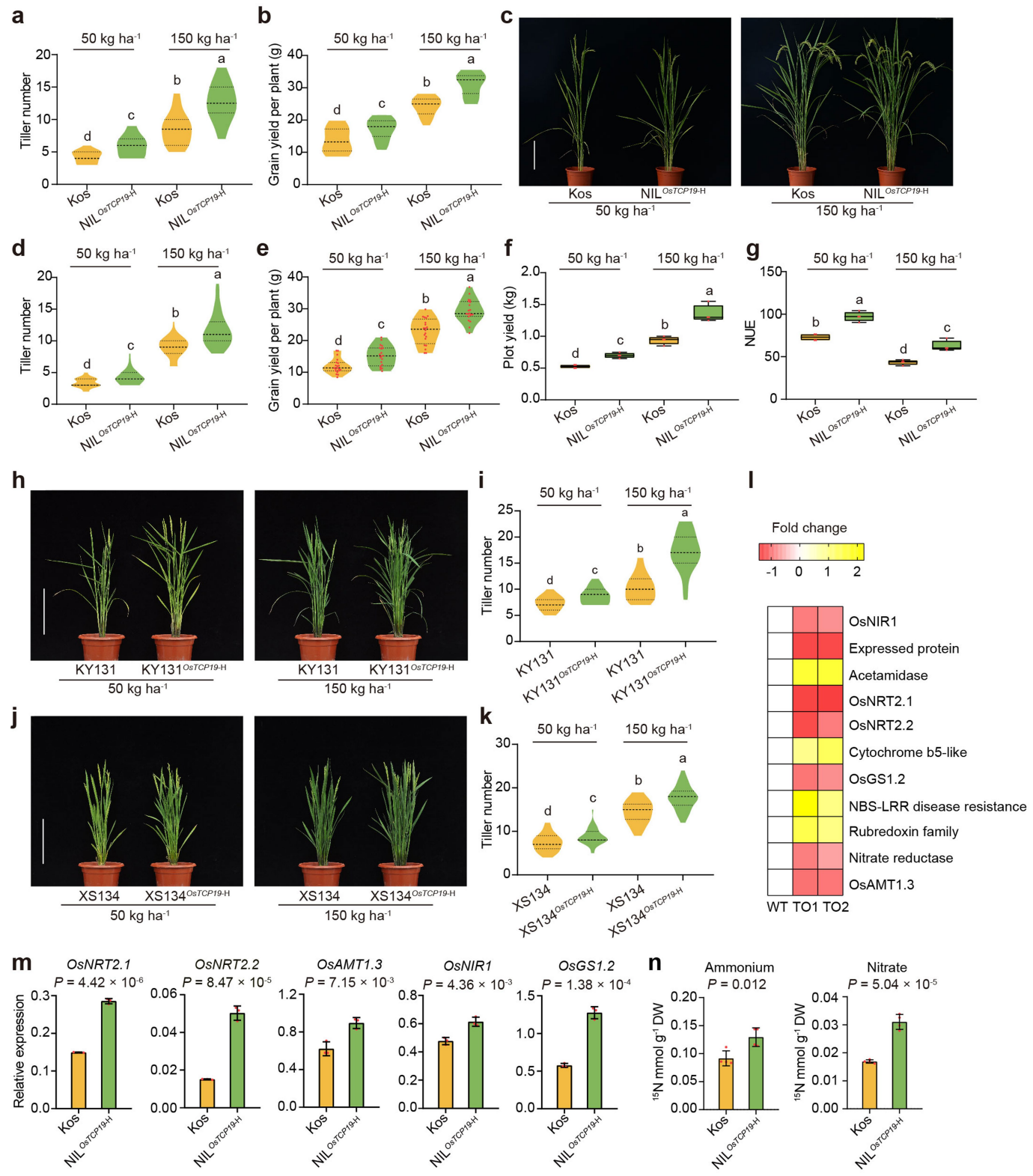
seedlings were collected and the 1st to 12th tiller buds of each seedling were analysed. **e**, Expression analysis of cell-cycle marker genes in ZH11, TO2 and *dlt* plants by qRT–PCR. Data are mean \pm s.d. ($n = 3$ biologically independent samples). Different letters indicate significant differences at $P < 0.05$ according to one-way ANOVA and Tukey's HSD test. For P values, see Source Data. **f**, Phenotype of ZH11, TO2 and *dlt* seedlings with or without 1 μ M brassinolide treatment. Scale bars, 8 cm. **g**, Statistical analysis of tiller number per plant of ZH11, TO2 and *dlt* plants. Data are mean \pm s.e.m. ($n = 6$ plants). Significant difference was determined by the two-sided Student's *t*-test. NS, not significant.



Extended Data Fig. 9 | *OsTCP19-H* negatively correlates with soil nitrogen content under the similar atmospheric temperature or precipitation conditions. **a**, Soil total nitrogen content variation in 29 countries or regions with similar mean annual temperature ($>25^{\circ}\text{C}$). **b**, *OsTCP19-H* negatively correlates with soil nitrogen content in the 29 countries or regions in **a**. **c**, Soil

total nitrogen content variation in 37 countries or regions with similar annual precipitation ($>800 \text{ mm}$). **d**, *OsTCP19-H* negatively correlates with soil nitrogen content in the 37 countries or regions in **c**. In **b**, **d**, data are average \pm s.d. ($n=4$ soil layers), and *P* values are determined by the two-sided Pearson correlation coefficient analysis.

Article



Extended Data Fig. 10 | See next page for caption.

Extended Data Fig. 10 | *OstCP19-H* increases crop yield and NUE of modern cultivars.

a, b, Statistical analysis of tiller number (**a**) ($n=22$ plants) and grain yield per plant (**b**) ($n=20$ plants) of Kos and NIL^{*OstCP19-H*} plants under two nitrogen conditions in Beijing in 2017. **c,** Phenotype of Kos and NIL^{*OstCP19-H*} plants grown under two nitrogen conditions in Beijing in 2018. Scale bar, 24 cm. **d–g,** Statistical analysis of Kos and NIL^{*OstCP19-H*} plants grown under two nitrogen conditions in field tests in Beijing in 2018. Tiller number (**d**) ($n=54$ plants), grain yield per plant (**e**) ($n=20$ plants), plot yield (**f**) ($n=4$ plots) and NUE (**g**) ($n=4$ plots) of Kos and NIL^{*OstCP19-H*} plants under two nitrogen conditions. **h,** Phenotype of Kongyu131 (KY131) and KY131^{*OstCP19-H*} plants under two nitrogen conditions. Scale bar, 24 cm. **i,** Statistical analysis of tiller number shown in **h** ($n=50$ plants). **j,** Phenotype of Xiushui134 (XS134) and XS134^{*OstCP19-H*} plants under two nitrogen conditions. Scale bar, 24 cm. **k,** Statistical analysis of tiller number shown in **j** ($n=50$ plants). **l,** A heat map of DEGs involved in nitrogen metabolism pathway (Kyoto Encyclopedia of Genes and Genomes, ko00910).

The colour key (red to yellow) represents gene expression (FPKM) as \log_2 -transformed fold changes of (TO1/WT) or (TO2/WT). The gene-encoding proteins are shown on the right. **m,** qRT-PCR-based transcript abundance analysis of *OsNRT2.1*, *OsNRT2.2*, *OsAMT1.3*, *OsNRI1* and *OsGS1.2* in Kos and NIL^{*OstCP19-H*} plants. Data are mean \pm s.d. ($n=3$ biologically independent samples). **n,** ¹⁵N accumulation in roots of Kos and NIL^{*OstCP19-H*} plants. ¹⁵N-nitrate and ¹⁵N-ammonium were used for ¹⁵N labelling in Kos and NIL^{*OstCP19-H*} plants, respectively. DW, dry weight. Data are mean \pm s.d. ($n=4$ biologically independent samples). In **a, b, d, e, i, k,** the bars in the violin plots represent 25th percentiles, medians, and 75th percentiles. **f, g,** The horizontal bars of boxes represent minima, 25th percentiles, medians, 75th percentiles and maxima. In **a, b, d–g, i, k,** different letters indicate significant differences at $P<0.05$ according to one-way ANOVA and Tukey's HSD test. For P values, see Source Data. In **m, n,** significant difference was determined by the two-sided Student's *t*-test.

Reporting Summary

Nature Research wishes to improve the reproducibility of the work that we publish. This form provides structure for consistency and transparency in reporting. For further information on Nature Research policies, see [Authors & Referees](#) and the [Editorial Policy Checklist](#).

Statistical parameters

When statistical analyses are reported, confirm that the following items are present in the relevant location (e.g. figure legend, table legend, main text, or Methods section).

n/a Confirmed

- The exact sample size (n) for each experimental group/condition, given as a discrete number and unit of measurement
- An indication of whether measurements were taken from distinct samples or whether the same sample was measured repeatedly
- The statistical test(s) used AND whether they are one- or two-sided
Only common tests should be described solely by name; describe more complex techniques in the Methods section.
- A description of all covariates tested
- A description of any assumptions or corrections, such as tests of normality and adjustment for multiple comparisons
- A full description of the statistics including central tendency (e.g. means) or other basic estimates (e.g. regression coefficient) AND variation (e.g. standard deviation) or associated estimates of uncertainty (e.g. confidence intervals)
- For null hypothesis testing, the test statistic (e.g. F , t , r) with confidence intervals, effect sizes, degrees of freedom and P value noted
Give P values as exact values whenever suitable.
- For Bayesian analysis, information on the choice of priors and Markov chain Monte Carlo settings
- For hierarchical and complex designs, identification of the appropriate level for tests and full reporting of outcomes
- Estimates of effect sizes (e.g. Cohen's d , Pearson's r), indicating how they were calculated
- Clearly defined error bars
State explicitly what error bars represent (e.g. SD, SE, CI)

Our web collection on [statistics for biologists](#) may be useful.

Software and code

Policy information about [availability of computer code](#)

Data collection

Bio-Rad CFX Manager v3.1 (qPCR data); ImageJ v1.49 (Lamina inclination measurement); Leica TCS SP5 (Subcellular localization); Leica RM2145, Leica DMR, and Apogee Instruments (histological analysis); BGISEQ-500 sequencer (RNA-seq data); 3K Rice Genomes Project (genomic data of Rice 3K population); GSD and HYDE v3.2.1 (soil nitrogen data); CRU TS v3.23 (climate data).

Data analysis

Microsoft Excel 2016, GraphPad Prism v8.0.1, and R v3.6.1 (two-sided Student's t-test, ANOVA, and Tukey's HSD test); GEMMA v0.941, PLINK v1.9, and ANGSD v0.931 (GWAS); R v3.6.1 and DESeq2 v1.26.0 (RNA-seq analysis); FIMO v5.2.0 (motif analysis of OsTCP19 promoter); ngsTools software and Beagle v3.3.2 (haplotype analysis of OsTCP19); Matlab R2016b (map of soil nitrogen content).

For manuscripts utilizing custom algorithms or software that are central to the research but not yet described in published literature, software must be made available to editors/reviewers upon request. We strongly encourage code deposition in a community repository (e.g. GitHub). See the Nature Research [guidelines for submitting code & software](#) for further information.

Data

Policy information about [availability of data](#)

All manuscripts must include a [data availability statement](#). This statement should provide the following information, where applicable:

- Accession codes, unique identifiers, or web links for publicly available datasets
- A list of figures that have associated raw data
- A description of any restrictions on data availability

The raw sequencing dataset of Rice Mini-Core Collection is available on NCBI BioProject (<https://www.ncbi.nlm.nih.gov/bioproject>) under the accession number PRJNA301661. The RNA-sequencing data have been deposited in NCBI's Gene Expression Omnibus (www.ncbi.nlm.nih.gov/geo/) under accession number GSE161265. Data of 3K Rice Genomes Project can be downloaded from Rice SNP-Seek Database (<https://snp-seek.irri.org/>). Soil nitrogen content data are available from Global Soil Dataset (GSD) (<http://globalchange.bnu.edu.cn>). The data of rice planting area of different countries are from the History Database of the Global Environment (HYDE 3.2.1) (<https://doi.org/10.17026/dans-25g-gez3>). Climate data are available from the Climatic Research Unit (CRU TS v. 3.23) (https://crudata.uea.ac.uk/cru/data/hrg/cru_ts_3.23/cruts.1506241137.v3.23/). The basemap in Fig. 1a was downloaded from <https://www.R-project.org/>. The basemap in Fig. 5a was downloaded from the ArcGIS Hub (https://hub.arcgis.com/datasets/a21fdb46d23e4ef896f31475217cbb08_1 (2020.11.01)).

Field-specific reporting

Please select the best fit for your research. If you are not sure, read the appropriate sections before making your selection.

Life sciences Behavioural & social sciences Ecological, evolutionary & environmental sciences

For a reference copy of the document with all sections, see nature.com/authors/policies/ReportingSummary-flat.pdf

Life sciences study design

All studies must disclose on these points even when the disclosure is negative.

Sample size	No statistical methods were used to predetermine sample size. For agronomic traits in the field, sample sizes were chosen based on our previous study (Hu et al., Nat. Genet. 2015, 47: 834-838). For tiller buds analysis and BL treatment, sample sizes were determined according to research in the field (Fang et al., Mol. Plant 2020, 13: 586-597).
Data exclusions	No data was excluded from the analyses.
Replication	All experiments in this study were repeated independently at three times. For qRT-PCR, three biologically independent samples were used each time. For subcellular localization, histological analysis of shoot base, and EMSA, the results are representative of three independent experiments. This information is shown in figure legends.
Randomization	All samples were arranged randomly into experimental groups.
Blinding	For molecular biology experiments, bias could not be introduced since samples were treated identically and collected randomly. Blind was not possible as the author who performed the experiment also analyzed the data. Investigation of agronomic traits and RNA-seq analysis were performed without prior knowledge of the result, blind was not applied.

Reporting for specific materials, systems and methods

Materials & experimental systems

n/a	Involved in the study
<input type="checkbox"/>	<input checked="" type="checkbox"/> Unique biological materials
<input type="checkbox"/>	<input checked="" type="checkbox"/> Antibodies
<input checked="" type="checkbox"/>	<input type="checkbox"/> Eukaryotic cell lines
<input checked="" type="checkbox"/>	<input type="checkbox"/> Palaeontology
<input checked="" type="checkbox"/>	<input type="checkbox"/> Animals and other organisms
<input checked="" type="checkbox"/>	<input type="checkbox"/> Human research participants

Methods

n/a	Involved in the study
<input type="checkbox"/>	<input checked="" type="checkbox"/> ChIP-seq
<input type="checkbox"/>	<input checked="" type="checkbox"/> Flow cytometry
<input checked="" type="checkbox"/>	<input type="checkbox"/> MRI-based neuroimaging

Unique biological materials

Policy information about [availability of materials](#)

Obtaining unique materials No restrictions on the availability of obtaining unique materials.

Antibodies

Antibodies used

Anti-FLAG (Sigma, F1804, 1:300 dilution for ChIP)

Validation

The Anti-FLAG M2 mouse, affinity purified monoclonal antibody binds to fusion proteins containing a FLAG peptide sequence. The antibody recognizes the FLAG peptide sequence at the N-terminus, Met-N-terminus,C-terminus, and internal sites of the fusion protein. The antibody is commercially available from the manufacturer. For more details about this product and the relevant citation, please see <https://www.sigmaldrich.com/catalog/product/sigma/f1804?lang=zh®ion=CN>